J|A|C|S
ARTICLES
Published on Web 10/16/2002

Steric and Electronic Effects on the Reactivity of Rh and Ir Complexes Containing P−S, P−P, and P−O Ligands. Implications for the Effects of Chelate Ligands in Catalysis

Luca Gonsalvi,[†,‡] Harry Adams,[‡] Glenn J. Sunley,[§] Evert Ditzel,[§] and Anthony Haynes*[,‡]

Contribution from the Department of Chemistry, University of Sheffield, Sheffield S3 7HF, U.K., and Hull Research and Technology Centre, BP Chemicals Ltd., Saltend, Hull HU12 8DS, U.K.

Received November 27, 2001

Abstract: Kinetic studies of the reactions of [M(CO)(L−L)I] [M = Rh, Ir; L−L = $Ph_2PCH_2P(S)Ph_2$ (dppms), $Ph_2PCH_2CH_2PPh_2$ (dppe), and $Ph_2PCH_2P(O)Ph_2$ (dppmo)] with methyl iodide have been undertaken. All the chelate ligands promote oxidative addition of methyl iodide to the square planar M(I) centers, by factors of between 30 and 50 compared to the respective $[M(CO)_2I_2]^-$ complexes, due to their good donor properties. Migratory CO insertion in [Rh(CO)(L−L)I_2Me] leads to acetyl complexes [Rh(L−L)I_2(COMe)] for which X-ray crystal structures were obtained for L−L = dppms (**3a**) and dppe (**3b**). Against the expectations of simple bonding arguments, methyl migration is faster by a factor of ca. 1500 for [Rh(CO)(dppms)I_2Me] (**2a**) than for [Rh(CO)(dppe)I_2Me] (**2b**). For M = Ir, alkyl iodide oxidative addition gives stable alkyl complexes [Ir(CO)(L−L)I_2R]. Migratory insertion (induced at high temperature by CO pressure) was faster for [Ir(CO)(dppms)I_2Me] (**5a**) than for its dppe analogue (**5b**). Reaction of methyl triflate with [Ir(CO)(dppms)I] (**4a**) yielded the dimer $[\{Ir(CO)(dppms)(\mu\text{-}I)Me\}_2]^{2+}$ (**7**), which was characterized crystallographically along with **5a** and [Ir(CO)(dppms)I_2Et] (**6**). Analysis of the X-ray crystal structures showed that the dppms ligand adopts a conformation which creates a sterically crowded pocket around the alkyl ligands of **5a**, **6**, and **7**. It is proposed that this steric strain can be relieved by migratory insertion, to give a five-coordinate acetyl product in which the sterically crowded quadrants flank a vacant coordination site, exemplified by the crystal structure of **3a**. Conformational analysis indicates similarity between M(dppms) and $M_2(\mu$-dppm) chelate structures, which have less flexibility than M(dppe) systems and therefore generate greater steric strain with the "axial" ligands in octahedral complexes. Ab initio calculations suggest an additional electronic contribution to the migratory insertion barrier, whereby a sulfur atom *trans* to CO stabilizes the transition state compared to systems with phosphorus *trans* to CO. The results represent a rare example of the quantification of ligand effects on individual steps from catalytic cycles, and are discussed in the context of catalytic methanol carbonylation. Implications for other catalytic reactions utilizing chelating diphosphines (e.g., CO/alkene copolymerization and alkene hydroformylation) are considered.

Introduction

Ligand steric and electronic effects play key roles in determining organometallic reactivity trends and catalytic properties. For monodentate ligands, a number of quantitative parameters (e.g., Tolman's cone angle,[1] Giering's QALE method,[2] and Drago's ECW model[3]) are well-established. Several important homogeneous catalysts now utilize bidentate ligands for which the stereoelectronic properties are less well understood. The ligand *bite angle*[4,5] has been shown to be important, although the precise way in which the effect of the bite angle is transmitted to the active site of the metal complex is still a matter of some debate, with electronic and steric effects both contributing.[6] Attempts to quantify the steric requirements of diphosphine ligands have recently been made by Koide et al., who introduced the *pocket angle* concept,[7] and Angermund et al., who used an *accessible molecular surface* model.[8] Despite the large body of work in this area, the quantification of ligand effects on individual steps from catalytic cycles is quite rare. In this paper we report kinetic, crystallographic, and theoretical data which illuminate the steric and electronic factors influencing key steps in ligand-promoted catalytic methanol carbonylation.

* Address correspondence to this author. E-mail: a.haynes@sheffield.ac.uk.
† Current address: Institute for the Chemistry of Organometallic Compounds, National Research Council (ICCOM-CNR), Via J Nardi 39-41, 50132 Firenze, Italy.
‡ University of Sheffield.
§ BP Chemicals Ltd.

(1) Tolman, C. A. *Chem. Rev.* **1977**, *77*, 313.
(2) Wilson, M. R.; Liu, H.; Prock, A.; Giering, W. P. *Organometallics* **1993**, *12*, 2044.
(3) Joerg, S.; Drago, R. S.; Sales, S. *Organometallics* **1998**, *17*, 589.
(4) Casey, C. P.; Whiteker, G. T. *Isr. J. Chem.* **1990**, *30*, 299.
(5) Dierkes, P.; van Leeuwen, P. W. N. M. *J. Chem. Soc., Dalton Trans.* **1999**, 1519. van Leeuwen, P. W. N. M.; Kamer, P. C. J.; Reek, J. N. H.; Dierkes, P. *Chem. Rev.* **2000**, *100*, 2741.
(6) Casey, C. P.; Paulsen, E. L.; Beuttenmueller, E. W.; Proft, B. R.; Petrovich, L. M.; Matter, B. A.; Powell, D. R. *J. Am. Chem. Soc.* **1997**, *119*, 11817.
(7) Koide, Y.; Bott, S. G.; Barron, A. R. *Organometallics* **1996**, *15*, 2213.
(8) Angermund, K.; Baumann, W.; Dinjus, E.; Fornika, R.; Görls, H.; Kessler, M.; Krüger, C.; Leitner, W.; Lutz, F. *Chem.—Eur. J.* **1997**, *3*, 755.

Scheme 1. Cycle for Methanol Carbonylation Catalyzed by **1a**

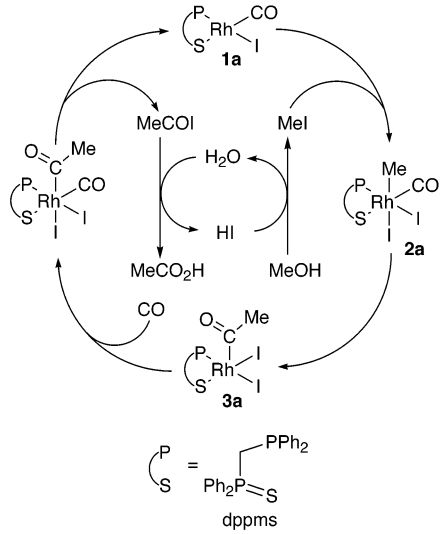

The findings are related to the behavior of other catalytic systems which use bidentate phosphine ligands.

Our studies were inspired by the findings of Baker et al.,[9,10] who reported an 8-fold enhancement in the rate of rhodium/iodide-catalyzed methanol carbonylation (at 185 °C and 70 bar of CO) on addition of the mixed P,S donor ligand $Ph_2PCH_2P(S)Ph_2$ (dppms). Mixed P,S[11] and P,O[12] ligands have been employed previously for the Rh/iodide-catalyzed carbonylation of methanol to acetic acid. Whereas $Ph_2PCH_2CH_2P(O)Ph_2$ (dppeo) was reported[12] to be an effective promoter for methanol carbonylation under relatively mild conditions (80 °C, ∼3 bar of CO), it gave only a marginal rate improvement under the more commercially relevant conditions employed by Baker et al. Likewise, $Ph_2PCH_2P(O)Ph_2$ (dppmo) and $Ph_2PN(Ph)P(S)Ph_2$ did not prove to be good promoters at 185 °C.

Preliminary mechanistic studies[10] identified the active species in the dppms-promoted system as the Rh(I) chelate complex [Rh(CO)(dppms)I] (**1a**), which was the only species observed by in situ high-pressure IR spectroscopy under catalytic conditions. The promotion is not therefore due to iodide salts formed by quaternization of the dppms ligand. The proposed catalytic cycle (Scheme 1) closely resembles the well-known Monsanto system[13] based on the anionic complex $[Rh(CO)_2I_2]^-$. A first-order dependence of catalytic rate on [MeI] was consistent with rate-determining oxidative addition of MeI to **1a** to give the methyl intermediate $[Rh(CO)(dppms)I_2Me]$ (**2a**). The stoichiometric reaction of **1a** with MeI, in the absence of CO, yielded the stable acetyl complex $[Rh(dppms)I_2(COMe)]$ (**3a**), resulting from facile migratory insertion in **2a**. Coordination of CO and reductive elimination of acetyl iodide completes the organometallic cycle. All the observed catalytic intermediates retain the Rh(dppms) chelate structure, in contrast with the dppeo-promoted system, where despite the much lower CO pressure, the sole observed species was $[Rh(CO)_2(dppeo)I]$ containing a monodentate P-coordinated dppeo ligand.[12]

Our investigation has been directed at quantifying the kinetics of oxidative addition and migratory insertion in the (dppms)Rh system, and comparing the rates with corresponding reactions of Rh complexes containing dppmo and $Ph_2P(CH_2)_2PPh_2$ (dppe), each of which also forms five-membered chelate rings. Bidentate phosphines $Ph_2P(CH_2)_nPPh_2$ ($n = 1-4$) are known to promote the reductive carbonylation (using a CO/H_2 mixture) of methanol to acetaldehyde and derivatives.[14] A range of symmetrical and unsymmetrical derivatives of dppe, containing fluorinated substituents on the phenyl rings, have recently been tested for acetic acid production, but all were found to be less active than the conventional $[Rh(CO)_2I_2]^-$-catalyzed system.[15]

In addition to our kinetic studies on the rhodium systems, we have made comparative measurements on some analogous iridium complexes, where oxidative addition generally gives stable alkyl complexes. A crystallographic study of $[Ir(CO)(dppms)I_2Me]$ (**5a**), an iridium model for the reactive intermediate **2a**, provides an insight into the steric effects on reactivity in these systems. Other X-ray crystal structures are presented which support the importance of steric effects in accelerating migratory insertion, while ab initio quantum mechanical calculations suggest that electronic effects also contribute, particularly for complexes with S *trans* to CO. A preliminary account of some of the experimental results has been published.[16]

Although our study is primarily directed at complexes and reactions involved in catalytic methanol carbonylation, our observations are more generally applicable to ligand effects on organometallic and catalytic reactivity. This is exemplified by consideration of ligand effects in catalytic CO/alkene copolymerization and hydroformylation reactions.

Results and Discussion

Synthesis of Rh(I) and Ir(I) Complexes [M(CO)(L−L)I]. The square planar rhodium(I) complexes [Rh(CO)(dppms)I] (**1a**), [Rh(CO)(dppe)I] (**1b**), and [Rh(CO)(dppmo)I] (**1c**) were synthesized by reaction of the dimeric precursor $[Rh(CO)_2I]_2$ with the appropriate bidentate ligand (eq 1). Spectroscopic

$$^1/_2[Rh(CO)_2I]_2 + L-L \rightarrow [Rh(CO)(L-L)I] + CO \quad (1)$$

parameters for the dppe complex **1b** were in accordance with the literature data reported by Moloy and Wegman.[14] For the dppms and dppmo complexes, there exists the possibility of two geometrical isomers with CO coordinated either *cis* or *trans* to the coordinated S or O heteroatom of the bidentate ligand. The ^{31}P NMR data indicate the presence of a single isomer in each case, and on the basis of similar spectroscopic data for the known chloride analogues [Rh(CO)(dppms)Cl][10] and [Rh(CO)(dppmo)Cl],[12] for which X-ray crystal structures have been determined, we assign the stereochemistry with CO *trans* to S or O. This geometry is reflected in the infrared spectra, which exhibit ν(CO) bands at relatively low frequency for **1a** (1987 cm^{-1}) and **1c** (1983 cm^{-1}) compared to **1b** (2011 cm^{-1}). The

(9) Baker, M. J.; Dilworth, J. R.; Sunley, J. G.; Wheatley, N. European Patent Application 632,006, 1995.
(10) Baker, M. J.; Giles, M. F.; Orpen, A. G.; Taylor, M. J.; Watt, R. J. *J. Chem. Soc., Chem. Commun.* **1995**, 197.
(11) Cavell, R. G. PCT Patent Application WO 92/04118, 1992. Dilworth, J. R.; Miller, J. R.; Wheatley, N.; Baker, M. J.; Sunley, J. G. *J. Chem. Soc., Chem. Commun.* **1995**, 1579.
(12) Wegman, R. W.; Abatjoglou, A. G.; Harrison, A. M. *J. Chem. Soc., Chem. Commun.* **1987**, 1891.
(13) Dekleva, T. W.; Forster, D. *Adv. Catal.* **1986**, *34*, 81. Forster, D. *Adv. Organomet. Chem.* **1979**, *17*, 255. Maitlis, P. M.; Haynes, A.; Sunley, G. J.; Howard, M. J. *J. Chem. Soc., Dalton Trans.* **1996**, 2187.
(14) Moloy, K. G.; Wegman, R. W. *Organometallics* **1989**, *8*, 2883.
(15) Carraz, C. A.; Ditzel, E.; Orpen, A. G.; Ellis, D. D.; Pringle, P. G.; Sunley, G. J. *Chem. Commun.* **2000**, 1277.
(16) Gonsalvi, L.; Adams, H.; Sunley, G. J.; Ditzel, E.; Haynes, A. *J. Am. Chem. Soc.* **1999**, *121*, 11233.

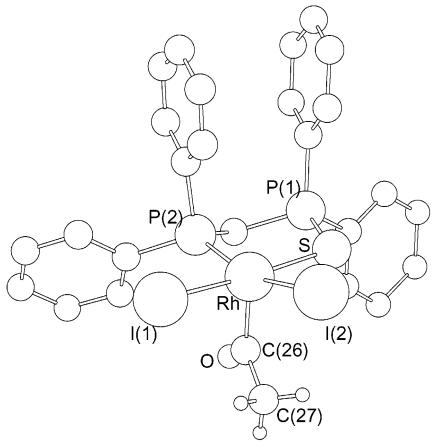

Figure 1. X-ray structure of [Rh(dppms)I_2(COMe)] (**3a**). Hydrogen atoms on the dppms ligand are omitted for clarity. Selected geometric data are given in Table 1.

shift in ν(CO) (and the preference for the observed geometry) is attributed to the ability of the coordinated S or O atoms to act as π (as well as σ) donors in **1a** and **1c** as opposed to the moderate π-acceptor PPh_2 moiety *trans* to CO in **1b**.

The iridium(I) complexes [Ir(CO)(dppms)I] (**4a**) and [Ir(CO)(dppe)I] (**4b**) were synthesized in the manner of Fisher and Eisenberg[17] by reaction of the anionic iridium precursor $Bu_4N[Ir(CO)_2I_2]$ with the appropriate bidentate ligand (eq 2).

$$Bu_4N[Ir(CO)_2I_2] + L{-}L \rightarrow [Ir(CO)(L{-}L)I] + CO + Bu_4NI \quad (2)$$

Spectroscopic data for **4b** were in accordance with literature values,[17] and data for the new dppms complex **4a** were consistent with the geometry displayed by the Rh analogue **1a** described above. The ν(CO) bands (1972 cm^{-1} for **4a** and 1994 cm^{-1} for **4b**) showed shifts of ca. 15 cm^{-1} to low frequency compared to those of the Rh complexes, reflecting the enhanced back-donating ability of the third-row metal. Attempts to synthesize the complex [Ir(CO)(dppmo)I] by a method similar to that used for **4a** and **4b** were unsuccessful.

Reactions of [M(CO)(L−L)I] with Methyl Iodide. The reaction of **1a** with excess methyl iodide leads smoothly to the acetyl product **3a**, which was fully characterized. When the reaction was performed at high [MeI], a weak ν(CO) band at 2062 cm^{-1} was observed in the IR spectrum in addition to the bands of **1a** and **3a**, consistent with the presence of a small amount of the intermediate methyl complex **2a**. The behavior of this intermediate is dealt with in more detail when the kinetics of this reactions are considered (vide infra). An X-ray crystal structure of **3a** (Figure 1) revealed a distorted square pyramidal geometry with an apical acetyl group. The methyl group of the acetyl ligand approaches an eclipsed conformation with respect to one of the basal iodides (dihedral angle C(27)−C(26)−Rh(1)−I(2) = 19°), which leads to I(2) being displaced from the ideal basal plane of the square pyramid (angle C(26)−Rh−I(2) = 105° compared with C(26)−Rh−I(1) = 92°). A very similar conformation of acetyl and iodide ligands is found in the structure of [Rh(dppp)I_2(COMe)] (dppp = $Ph_2P(CH_2)_3PPh_2$).[18,19]

(17) Fisher, E.; Eisenberg, R. *Inorg. Chem.* **1984**, *23*, 3216.
(18) Moloy, K. G.; Petersen, J. L. *Organometallics* **1995**, *14*, 2931.

Table 1. Selected Bond Lengths (Å) and Angles (deg) for Rhodium Acetyl Complexes **3a** and **3b**

3a		3b	
Rh−C(26)	1.951(6)	Rh−C(27)	2.013(7)
Rh−S	2.357(2)	Rh−P(1)	2.267(2)
Rh−P(2)	2.256(2)	Rh−P(2)	2.284(2)
Rh−I(1)	2.6497(19)	Rh−I(1)	2.7035(12)
Rh−I(2)	2.7024(19)	Rh−I(2)	2.7029(13)
O−C(26)	1.178(7)	O−C(27)	1.178(9)
C(26)−C(27)	1.491(9)	C(27)−C(28)	1.490(11)
P(1)−S	2.027(3)		
C(26)−Rh−S	93.62(19)	C(27)−Rh−P(1)	91.2(2)
C(26)−Rh−P(2)	92.80(19)	C(27)−Rh−P(2)	92.5(2)
C(26)−Rh−I(1)	92.23(18)	C(27)−Rh−I(1)	103.4(2)
C(26)−Rh−I(2)	104.84(19)	C(27)−Rh−I(2)	99.1(2)
P(2)−Rh−S	90.47(9)	P(1)−Rh−P(2)	84.74(7)
P(2)−Rh−I(1)	91.74(9)	P(2)−Rh−I(1)	90.73(6)
S−Rh−I(1)	173.64(4)	P(1)−Rh−I(1)	164.90(5)
P(2)−Rh−I(2)	161.77(4)	P(2)−Rh−I(2)	167.28(5)
S−Rh−I(2)	83.96(8)	P(1)−Rh−I(2)	89.80(6)
I(1)−Rh−I(2)	92.12(8)	I(2)−Rh−I(1)	91.62(4)
O−C(26)−C(27)	120.1(6)	O−C(27)−C(28)	123.4(7)
O−C(26)−Rh	123.8(5)	O−C(27)−Rh	124.5(6)
C(27)−C(26)−Rh	116.1(5)	C(28)−C(27)−Rh	112.1(5)

Scheme 2. Reaction of **1b** with Methyl Iodide and Isomers of **2b**[14]

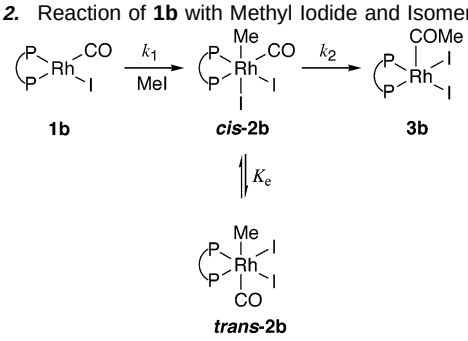

The reaction of the Rh(dppe) complex **1b** with methyl iodide has been reported previously, leading to [Rh(dppe)I_2(COMe)] (**3b**) via the relatively long-lived intermediate [Rh(CO)(dppe)I_2Me)] (**2b**), for which isomers with CO *cis* or *trans* to methyl were identified in solution by ^1H and ^{31}P NMR spectroscopy (Scheme 2).[14] Since the original report did not state the ratio of isomers observed, we have reproduced the ^{31}P NMR experiment (in CD_2Cl_2 containing 3.2 M CH_3I at ambient temperature) and found that the ratio *cis*-**2b**:*trans*-**2b** remains at ca. 2:3 for most of the duration of the experiment.[20] In the first spectrum recorded after addition of the methyl iodide, however, a slightly higher proportion of *cis*-**2b** was apparent (ratio *cis*-**2b**:*trans*-**2b** = ca. 4:5), suggesting that *cis*-**2b** is the kinetic product and that equilibrium between the two isomers is attained quite rapidly. A recent theoretical investigation predicted that the two isomers are virtually isoenergetic,[21] in agreement with our experimental observations. The mechanism for isomerization likely involves a five-coordinate intermediate formed by loss of a CO or iodide ligand or by dechelation of one arm of the dppe ligand. Our data do not distinguish these possibilities.

An X-ray crystal structure of the stable acetyl product **3b** (Figure 2) revealed a distorted square pyramidal geometry with the acetyl ligand in the apical position, similar to structures

(19) Søtofte, I.; Hjortkjaer, J. *Acta Chem. Scand.* **1994**, *48*, 872.
(20) ^{31}P NMR resonances were observed for *cis*-**2b** at δ 36.2 (dd, J_{RhP} = 103 Hz) and 61.1 (dd, J_{RhP} = 115 Hz, J_{PP} = 14 Hz) and *trans*-**2b** at δ 56.2 (d, J_{RhP} = 120 Hz), in agreement with the data reported in ref 14.
(21) Cavallo, L.; Sola, M. *J. Am. Chem. Soc.* **2001**, *123*, 12294.

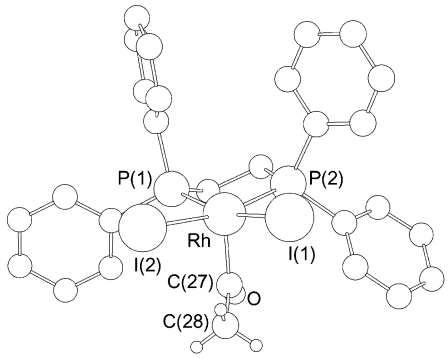

Figure 2. X-ray structure of [Rh(dppe)I_2(COMe)] (**3b**). Hydrogen atoms on the dppe ligand are omitted for clarity. Selected geometric data are given in Table 1.

reported previously for other [Rh(L−L)I_2(COMe)] complexes (L−L = $Ph_2PCH_2PPh_2$, dppm,[22] and dppp[18,19]). In **3b**, the plane of the acetyl ligand approximately bisects the I−Rh−I angle and the two C_{acetyl}−Rh−I bond angles (103° and 99°) show less asymmetry than the corresponding angles in **3a**.

The reaction of the Rh(dppmo) complex **1c** with methyl iodide (1.2−3.2 M, large excess) in CH_2Cl_2 gave an equilibrium mixture of methyl and acetyl products indicated in the IR spectrum by a terminal ν(CO) band at 2057 cm^{-1} for **2c** and a series of bands in the acetyl region at 1704, 1673, and 1651 cm^{-1}, presumably due to isomers or conformers of **3c**. No pure product was isolated from this mixture. The ^{31}P NMR spectrum of a solution of **1c** dissolved in CD_2Cl_2 containing MeI (20-fold excess) showed the presence of **1c** together with signals at δ 67.3 (dd, $^2J_{RhP}$ = 4 Hz) and 47.8 (dd, $^1J_{RhP}$ = 107 Hz, $^2J_{PP}$ = 20 Hz), which we assign to the acetyl complex [Rh(dppmo)I_2-(COMe)] (**3c**). An IR spectrum of the residue from this NMR experiment confirmed the presence of **1c** and **3c** as the major species along with a small amount of the methyl complex **2c**, which was not detected by NMR. After exposure of the solution to CO (1 atm) for 1 h the ^{31}P NMR spectrum showed the presence of another species, with signals at δ 45.1 (d) and 21.3 (dd, $^1J_{RhP}$ = 127 Hz, $^2J_{PP}$ = 11 Hz, $^2J_{RhP}$ not resolved) attributed to [Rh(CO)(dppmo)I_2(COMe)], by analogy with the pattern reported in the literature for the dppms analogue.[10]

When the reaction of **1c** with methyl iodide was carried out in acetonitrile, a much smaller amount of the methyl complex **2c** was observed in the IR spectrum, together with an increased proportion of acetyl product which displayed two ν(CO) bands at 1663 and 1685 cm^{-1} rather than the three bands observed in CH_2Cl_2. A ^{31}P NMR experiment in CD_3CN showed a product with signals at δ 42.9 (d) and 29.0 (dd, $^1J_{RhP}$ = 148 Hz, $^2J_{PP}$ = 7 Hz), and an IR spectrum of this species displayed the same pair of ν(CO) bands in the acetyl region. This suggests that migratory insertion in **2c** is promoted by coordination of acetonitrile to the five-coordinate acetyl product **3c** to give isomers of the solvento species [Rh(dppmo)(NCMe)I_2(COMe)] (**3c**−**MeCN**). A crystal structure of this complex (Supporting Information) shows a structure with *trans* iodides and the acetyl ligand *trans* to the oxygen atom of the dppmo chelate, with a molecule of acetonitrile coordinated *trans* to phosphorus.

The iridium(I) dppms complex **4a** reacts with methyl iodide to give a stable methyl complex, **5a**, which does not undergo spontaneous migratory insertion. Spectroscopic data for **5a** indicate the presence of two isomers in solution, in the approximate ratio 3:1. An X-ray crystal structure (Figure 3) showed a single isomer in the solid state, with methyl *cis* to both P and S donor atoms from the chelate and CO *trans* to sulfur. A solution of crystals from the batch used for the X-ray study gave a ^{31}P NMR spectrum identical to that of the major isomer of the bulk product, allowing us to assign the geometry of this species as that found in the crystal structure. The methyl ligands of both isomers each display ^{1}H resonances with a relatively weak coupling to phosphorus ($^3J_{HP}$ = 4 Hz) showing that methyl is *cis* to coordinated P in each case. This leaves four possible geometries for the minor isomer of **5a**, which our data do not distinguish. Complex **4a** was also found to react with ethyl iodide to give a stable ethyl complex, [Ir(CO)I_2-(dppms)Et] (**6**). Again the solution NMR data showed the presence of two isomers in the approximate ratio 3:1. An X-ray crystal structure (Figure 4) indicated a single isomer in the solid state with a coordination geometry about the iridium center corresponding to that in the methyl analogue **5a**. The reaction of the Ir(dppe) complex **4b** with methyl iodide to give [Ir(CO)-(dppe)I_2Me)] (**5b**) (including an X-ray crystal structure of **5b**) has been reported by Cleary and Eisenberg.[23−25] Their data are

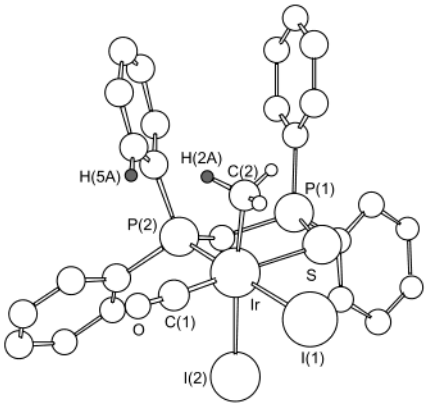

Figure 3. X-ray structure of [Ir(CO)(dppms)I_2Me] (**5a**). Selected hydrogen atoms on the dppms ligand are omitted for clarity. Selected geometric data are given in Table 2.

Table 2. Selected Bond Lengths (Å) and Angles (deg) for Iridium Alkyl Complexes **5a**, **6**, and **7**

	5a	6	7
Ir−C(2)	2.143(5)	2.175(8)	2.130(5)
Ir−C(1)	1.867(4)	1.826(9)	1.878(5)
Ir−S	2.4194(9)	2.416(2)	2.4182(13)
Ir−P(2)	2.2923(10)	2.284(2)	2.2949(12)
Ir−I(1)	2.7340(4)	2.7173(6)	2.7222(4)
Ir−I(2)	2.7935(4)	2.8086(6)	2.7890(4)
P(1)−S	2.0126(13)	2.009(3)	2.0138(18)
O−C(1)	1.126(5)	1.167(11)	1.135(6)
C(2)−Ir−P(2)	96.43(11)	94.0(2)	97.23(15)
C(2)−Ir−S	86.31(11)	84.0(2)	86.69(15)
C(2)−Ir−I(1)	86.56(10)	85.3(2)	86.50(14)
C(1)−Ir−C(2)	90.74(16)	93.2(3)	94.5(2)
P(2)−Ir−S	91.32(3)	89.99(7)	93.16(4)
C(1)−Ir−P(2)	94.24(12)	95.5(2)	93.41(16)
C(1)−Ir−I(1)	89.78(12)	87.7(2)	89.94(15)
S−Ir−I(1)	84.79(2)	86.82(5)	83.37(3)
O−C(1)−Ir	176.6(4)	178.1(8)	175.7(5)

(22) Adams, H.; Bailey, N. A.; Mann, B. E.; Manuel, C. P. *Inorg. Chim. Acta* **1992**, *198*−*200*, 111.
(23) Cleary, B. P.; Eisenberg, R. *Inorg. Chim. Acta* **1995**, *240*, 135.
(24) Cleary, B. P. Ph.D. Thesis, University of Rochester, Rochester, NY, 1995.

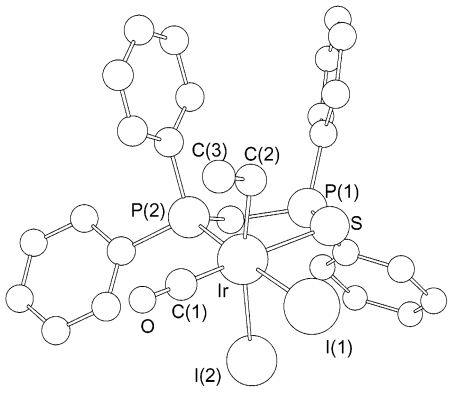

Figure 4. X-ray structure of [Ir(CO)(dppms)I_2Et] (**6**). Hydrogen atoms are omitted for clarity. Selected geometric data are given in Table 2.

Scheme 3. General Scheme for Reactions of [M(CO)(L−L)I] with Methyl Iodide[a]

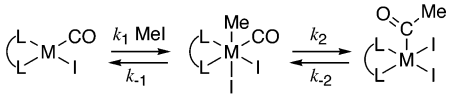

1a-c M = Rh
4a,b M = Ir

2a-c M = Rh
5a,b M = Ir

3a-c M = Rh

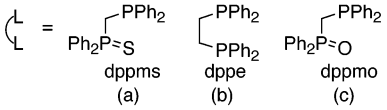

[a] Alternative isomers of methyl complexes **2** and **5** are omitted for simplicity.

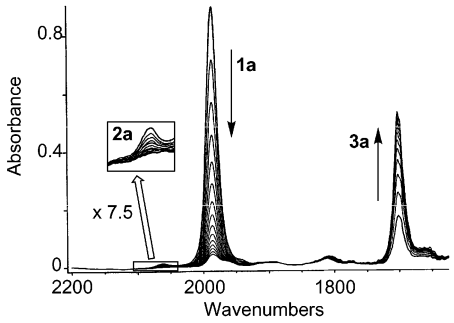

Figure 5. Series of IR spectra for the reaction of **1a** with MeI (8 M in CH_2Cl_2,10 °C). Note the weak band due to intermediate **2a**.

in agreement with ours and show that **5b** is formed as a single isomer with inequivalent phosphorus atoms and methyl *trans* to iodide, analogous to the Rh isomer *cis*-**2b** (Scheme 2).[14]

Kinetics of Methyl Iodide Oxidative Addition to [M(CO)(L−L)I]. Kinetic measurements for the reactions of **1a**−**c**, **4a**, and **4b** with methyl iodide in CH_2Cl_2 were carried out using IR spectroscopy to monitor changes in the ν(CO) bands due to reactants, intermediates (where possible), and products. A generalized reaction scheme is given in Scheme 3. Typical series of spectra for the reactions of the rhodium complexes **1a**−**c** are shown in Figures 5−7. Pseudo-first-order conditions were employed (at least 10-fold excess MeI), and in all cases, the disappearance of [M(CO)(L−L)I] was found to be first-order in both [complex] and [MeI]. Observed pseudo-first-order rate constants (k_{obs}) are given in the Supporting Information, and

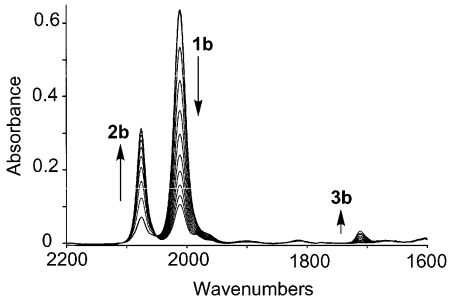

Figure 6. Series of IR spectra for the reaction of **1b** with MeI (1.6 M in CH_2Cl_2, 25 °C).

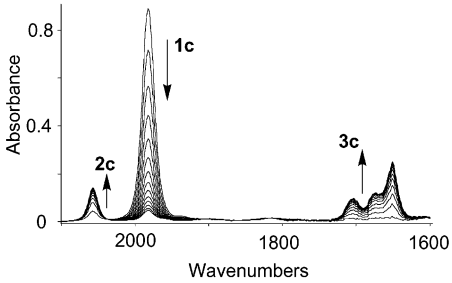

Figure 7. Series of IR spectra for the reaction of **1c** with MeI (1.6 M in CH_2Cl_2, 25 °C). The absorptions in the region 1650−1700 cm^{-1} are due to isomers or conformers of **3c**, in equilibium with **2c**.

Table 3. Rate Constants (25 °C) and Activation Parameters for Methyl Iodide Oxidative Addition Reactions in CH_2Cl_2

reactant	ν(XO), cm^{-1}	10^3k_1, $M^{-1}\,s^{-1}$	$\Delta H^{\ddagger}$, kJ mol^{-1}	$\Delta S^{\ddagger}$, J $mol^{-1}\,K^{-1}$
1a	1987	1.19	47 ± 1	−144 ± 2
1b	2011	1.41	40 ± 1	−167 ± 2
1c	1983	1.14	34 ± 4	−188 ± 13
[Rh(CO)(PEt_3)$_2$I][28]	1961	1.37	56 ± 13	−112 ± 44
$[Rh(CO)_2I_2]^-$ [29]	2059, 1988	0.0293	50 ± 1	−165 ± 4
4a	1972	50.0	34 ± 1	−156 ± 2
4b	1994	51.8	30 ± 1	−169 ± 3
$[Ir(CO)_2I_2]^-$ [30]	2045, 1969	3.12	54 ± 1	−113 ± 4

second-order rate constants (k_1) calculated from these are given in Table 3. Variable-temperature kinetic data over the range 10−35 °C were also measured, and satisfactory linear Eyring plots of these data gave the activation parameters listed in Table 3. In all cases the large negative activation entropies are consistent with the associative S_N2 mechanism commonly found for oxidative addition of methyl iodide to metal centers.[26,27]

The second-order rate constant for oxidative addition of MeI to **1a** (Table 3) represents a rate enhancement by a factor of ca. 41 at 25 °C compared to the Monsanto catalyst $[Rh(CO)_2I_2]^-$.[29] The activation parameters display a slightly lower $\Delta H^{\ddagger}$ and a more favorable $\Delta S^{\ddagger}$ than for oxidative addition of MeI to $[Rh(CO)_2I_2]^-$, resulting in a lowering of $\Delta G^{\ddagger}$ by ca. 10 kJ mol^{-1}. Very similar oxidative addition rates were found for the other Rh(I) complexes studied, with rate enhancements relative to $[Rh(CO)_2I_2]^-$ of 48 for **1b** and 35 for **1c**. The oxidative addition rates measured here are also comparable with the data reported by Rankin et al. for the monodentate phosphine-containing

(25) Albietz, P. J., Jr.; Cleary, B. P.; Paw, W.; Eisenberg, R. *Inorg. Chem.* **2002**, *41*, 2095.

(26) Fulford, A.; Hickey, C. E.; Maitlis, P. M. *J. Organomet. Chem.* **1990**, *398*, 311.

(27) Griffin, T. R.; Cook, D. B.; Haynes, A.; Pearson, J. M.; Monti, D.; Morris, G. E. *J. Am. Chem. Soc.* **1996**, *118*, 3029. Rendina, L. M.; Puddephatt, R. J. *Chem. Rev.* **1997**, *97*, 1735. Labinger, J. A.; Osborn, J. A. *Inorg. Chem.* **1980**, *19*, 3230.

complex *trans*-[Rh(CO)(PEt_3)$_2$I].[28] It is noteworthy that the complexes **1a**−**c** and *trans*-[Rh(CO)(PEt_3)$_2$I] all have similar nucleophilicity toward methyl iodide, varying by a factor of less than 1.5 in rate (or 1 kJ mol^{-1} in $\Delta G^{\ddagger}_{298}$) despite the relatively wide range (50 cm^{-1}) of ν(CO) frequencies for the four complexes. The ν(CO) values of metal carbonyl complexes are often taken as a good measure of electron density at the metal center, and so might be expected to be related to nucleophilicity. However, it is important to consider the local environment of the coordinated CO and, in particular, the *trans* ligand. For example, complex **1b** might be expected to have electron density on the Rh center rather similar to that of *trans*-[Rh(CO)(PPh_3)$_2$I], but the ν(CO) values are actually quite different (2011 and 1981 cm^{-1}, respectively) since a CO *trans* to iodide experiences considerably more back-donation than one *trans* to PPh_3. The use of ν(CO) to judge electron density on the metal should therefore be made with consideration of the stereochemistry of the complexes being compared.[31]

Halide salts have previously been found to accelerate MeI addition to square planar Rh(I)[26,32] and Ir(I)[33] complexes. Rate enhancements were also found for the complexes studied here (k_{obs} values are given in the Supporting Information). Addition of 1 equiv of Bu_4NI (per Rh) increased the oxidative addition rate by factors of ca. 1.3 (**1a**), 1.1 (**1b**), and 2.4 (**1c**), while 10 equiv of Bu_4NI gave rate enhancements of ca. 2.1 (**1a**), 1.6 (**1b**), and 8.1 (**1c**). It has been proposed previously that coordination of an additional halide ligand increases the nucleophilicity of the metal center. We have therefore probed the behavior of complexes **1a**−**1c** in the presence of excess ionic iodide. Addition of a 100-fold excess of Bu_4NI to solutions of **1a** or **1c** in CH_2Cl_2 did not give rise to any new rhodium carbonyl species detectable by IR spectroscopy. By contrast, under the same conditions the dppe complex **1b** gives rise (over 3 h) to significant amounts of a new species with ν(CO) at 1960 cm^{-1}. The shift of ν(CO) to low frequency is consistent with coordination of iodide to form an anionic complex, [Rh(CO)I_2(dppe)]$^-$. This complex could be five-coordinate (with the dppe ligand remaining bidentate) or square planar with one arm of the dppe ligand dissociating. We note that a phosphine ligand in [Rh(CO)I(PPh_3)$_2$] can be displaced by iodide to give an anionic complex, [Rh(CO)I_2(PPh_3)]$^-$ (ν(CO) 1963 cm^{-1}), which is more reactive toward MeI than the neutral precursor.[32] The iodide effects observed in our kinetic studies are best explained by iodide coordination to give reactive anionic intermediates, possibly accompanied by chelate ring opening.[34] The most facile dechelation would be expected for the dppmo chelate ligand, and the largest rate enhancement is indeed found for complex **1c**. Somewhat surprisingly though, no spectroscopic evidence for an anionic species was found in this case.

As expected, faster oxidative addition rates were found for the iridium complexes **4a** and **4b**. The ratios k_{Ir}/k_{Rh} were found to be 42 for the pair of dppms complexes and 37 for the pair of dppe complexes, corresponding to a $\Delta\Delta G^{\ddagger}_{298}$ of ca. 9 kJ mol^{-1} between Rh and Ir. A bigger difference in reactivity toward methyl iodide was found previously for the anionic iodocarbonyls [M(CO)$_2$I$_2$]$^-$, for which $k_{Ir}/k_{Rh} = 120$ corresponding to $\Delta\Delta G^{\ddagger}_{298} \approx 12$ kJ mol^{-1}.[30] The smaller difference in reactivity found between 4d and 5d metal complexes in this study can be ascribed to the presence of bulkier bidentate ligands which moderate the intrinsic nucleophilicity of the metal center. For all the oxidative addition reactions studied, addition of polar solvents (THF, MeCN, and MeOH) was found to give moderate rate enhancements (by factors of between 1 and 3; see the Supporting Information) as expected for S_N2 reactions proceeding via polar transition states. Coordination of solvent to the metal center during the S_N2 process may also play a role in accelerating oxidative addition.

Kinetics of Migratory CO Insertion in [M(CO)(L−L)I_2Me]. In the series of spectra for the reaction of **1a** with MeI (Figure 5), a weak absorption is apparent at 2062 cm^{-1} in addition to the bands at 1987 and 1701 cm^{-1} due to reactant **1a** and product **3a**, respectively. This weak band occurs in the region expected for the methyl intermediate **2a**, on the basis of the frequency shift (75 cm^{-1}) relative to the Rh(I) precursor **1a**.[35] A similar shift in ν(CO) (69 cm^{-1}) is found between the stable iridium analogues **4a** and **5a**. The kinetic behavior of the 2062 cm^{-1} band is also consistent with assignment to intermediate **2a**, since it decays in direct proportion to the band of **1a** as predicted by the steady-state approximation

$$\frac{d[\mathbf{2a}]}{dt} \approx 0 = k_1[\mathbf{1a}][\mathrm{MeI}] - k_{-1}[\mathbf{2a}] - k_2[\mathbf{2a}] \qquad (3)$$

$$\frac{[\mathbf{2a}]}{[\mathbf{1a}]} = \frac{k_1[\mathrm{MeI}]}{k_{-1} + k_2} \qquad (4)$$

Since k_{obs} is given by the expression

$$k_{obs} = \frac{k_1 k_2[\mathrm{MeI}]}{k_{-1} + k_2} \qquad (5)$$

eqs 4 and 5 can be combined to give

$$k_2 = \frac{k_{obs}}{[\mathbf{2a}]/[\mathbf{1a}]} \qquad (6)$$

The migratory insertion rate constant, k_2, can therefore be obtained from the measured value of k_{obs} and the steady-state ratio [**2a**]/[**1a**], which can be estimated on the basis of observed IR absorbances and estimated relative extinction coefficients for **1a** and **2a**.[36] Values of k_2 in the range 10−25 °C obtained

(28) Rankin, J.; Poole, A. D.; Benyei, A. C.; Cole-Hamilton, D. J. *Chem. Commun.* **1997**, 1835. Rankin, J.; Benyei, A. C.; Poole, A. D.; Cole-Hamilton, D. J. *J. Chem. Soc., Dalton Trans.* **1999**, 3771.
(29) Haynes, A.; Mann, B. E.; Morris, G. E.; Maitlis, P. M. *J. Am. Chem. Soc.* **1993**, *115*, 4093.
(30) Ellis, P. R.; Pearson, J. M.; Haynes, A.; Adams, H.; Bailey, N. A.; Maitlis, P. M. *Organometallics* **1994**, *13*, 3215.
(31) An empirical method of predicting ν(CO) values for metal complexes (Timney, J. A. *Inorg. Chem.* **1979**, *18*, 2502) takes this into account by utilizing different ligand effect constants depending upon whether the ligand is *cis* or *trans* to CO. The Timney method predicts ν(CO) values of 2006.6 and 1970.5 cm^{-1}, respectively, for the *cis* and *trans* isomers of [Rh(CO)(PPh_3)$_2$I], in agreement with the experimental trend.
(32) Forster, D. *J. Am. Chem. Soc.* **1975**, *97*, 951.
(33) Basson, S. S.; Leipoldt, J. G.; Purcell, W.; Schoeman, J. B. *Inorg. Chim. Acta* **1990**, *173*, 155. de Waal, D. J. A.; Gerber, T. I. A.; Louw, W. J. *Inorg. Chem.* **1982**, *21*, 1259.
(34) Our (unpublished) mechanistic studies of the reactions of [Rh(CO)I($Ph_2PCH_2CH_2PAr_2$)] (Ar = 3,5-$(CF_3)_2C_6H_3$ or 3,4,5-$F_3C_6H_2$) with MeI indicate that chelate ring opening and coordination of iodide is more facile in these complexes.
(35) Attempts to observe **2a** by low-temperature ^{31}P NMR were hampered by the low solubility of **1a** under these conditions.
(36) The band due to **2a** at 2062 cm^{-1} occurs under the high-frequency tail of the strong absorption of **1a** at 1987 cm^{-1}. The value of the ratio Abs(**2a**)/Abs(**1a**) at 8 M MeI was therefore obtained by plotting A(2062)/A(1987) vs [MeI] and subtracting the y intercept of the linear plot from the measured

Table 4. Rate Constants (25 °C, CH_2Cl_2) and Activation Parameters for Migratory Insertion Reactions of Rhodium Methyl Complexes

reactant	10^3k_2, s^{-1}	$\Delta H^{\ddagger}$, kJ mol^{-1}	$\Delta S^{\ddagger}$, J mol^{-1} K^{-1}
2a	620	54 ± 7	-67 ± 15
2b	0.4	83 ± 2	-30 ± 5
$[Rh(CO)_2I_3Me]^-$ [29]	54	63 ± 2	-59 ± 9

by this method are listed in the Supporting Information. Table 4 gives the value of k_2 at 25 °C together with activation parameters derived from an Eyring plot.

The series of spectra in Figure 6 show that a much higher concentration of methyl intermediate **2b** is formed during the reaction of **1b** with methyl iodide, as a consequence of a much slower migratory insertion step in the dppe system. Infrared spectroscopy does not distinguish between the *cis* and *trans* isomers of **2b** (Scheme 2), but ^{31}P NMR spectroscopy (vide supra) showed that a relatively fast equilibration leads to an isomeric ratio *cis*-**2b**:*trans*-**2b** of ca. 2:3 which remains steady during most of the experiment. Apparent rate constants for migratory insertion were obtained by monitoring the slow exponential decay of the combined ν(CO) band of *cis*- and *trans*-**2b** at 2075 cm^{-1} once the relatively rapid oxidative addition step was complete. The resulting rate constants (Supporting Information) were found to be essentially independent of [MeI]. An estimate of the true rate constant, k_2, for migratory insertion must take into account the proportion of **2b** existing in the *cis* form, since only that isomer possesses the appropriate geometry for *cis* migration.[37] On the basis of the mechanism shown in Scheme 2, and assuming that *cis*−*trans* isomerization is fast relative to migratory insertion, the observed rate constant is given by $k_2/(1 + K_e)$. Since ^{31}P NMR gave an estimate of $K_e = 1.5$, k_2 can be obtained by multiplying the observed rate constant by 2.5, leading to the value given in Table 4. The activation parameters for the reaction *cis*-**2b** → **3b** given in Table 4 were estimated with the approximation that K_e for the *cis*−*trans* isomerization is invariant with temperature.

Despite the indirect methods employed for obtaining these kinetic parameters, there is clearly a dramatic difference in reactivity between **2a** and **2b**, with the dppms complex undergoing migratory insertion ca. 1500 times faster than the dppe complex, corresponding to a lowering of $\Delta G^{\ddagger}_{298}$ by ca. 18 kJ mol^{-1}. Thus, while migratory insertion in **2a** is accelerated by an order of magnitude compared with that in $[Rh(CO)_2I_3Me]^-$, the reaction of **2b** is >10 times slower than for the conventional Monsanto catalyst.[29,38] By comparison, in the PEt_3 system studied by Rankin et al., it was found that migratory insertion only proceeded slowly when $[Rh(CO)(PEt_3)_2I_2Me]$ was subjected to a high pressure of carbon monoxide, which trapped the presumed five-coordinate intermediate to give $[Rh(CO)(PEt_3)_2I_2(COMe)]$.[28]

More complex behavior was exhibited by the dppmo system, where reaction of **1c** with MeI gave an equilibrium mixture of methyl and acetyl products **2c** and **3c** (Figure 7 and vide supra), which precluded the determination of accurate rate data for the migratory insertion step. However, since the IR bands due to the acetyl product **3c** grow-in simultaneously with those of the methyl intermediate **2c**, the equilibrium between **2c** and **3c** must be attained quite rapidly, indicating a relatively fast methyl migration. The replacement of sulfur by oxygen as the donor atom in the bidentate ligand therefore appears to affect the thermodynamics of migratory insertion more than the kinetics.

No spontaneous methyl migration was observed for **5a** and **5b**, in accordance with the behavior of other iridium(III) methyl complexes.[39] We therefore investigated the propensity for these complexes to undergo CO insertion by studying their reactions with carbon monoxide at high temperature and pressure. On the basis of previous observations for the anionic complex $[Ir(CO)_2I_3Me]^-$, we chose a solvent system comprising 1% (v/v) methanol in chlorobenzene.[40] When the reaction of **5a** with CO (10 bar) at 93 °C was followed by in situ high-pressure IR spectroscopy, the ν(CO) band of the reactant at 2039 cm^{-1} was replaced by a new terminal ν(CO) band at 2051 cm^{-1} in a first-order process ($k_{obs} = 7.3 \times 10^{-4}$ s^{-1}). Under the same conditions the rate constant for carbonylation of $[Ir(CO)_2I_3Me]^-$ is estimated as ca. 3×10^{-4} s^{-1}.[41] The recovered product showed IR bands at 2057 and 1642 cm^{-1} (CH_2Cl_2), consistent with a product containing terminal and acetyl CO ligands, and the ^{1}H and ^{31}P NMR spectra of this product gave evidence for two isomers in an approximate 1:1 ratio [$\delta(^1H)$ 2.59, 2.77; $\delta(^{31}P)$ 63.1, 4.5 (each d, $^2J_{PP} = 36$ Hz) and 56.3, −7.8 (each d, $^2J_{PP} = 25$ Hz)]. An X-ray crystal structure determination was hampered by disorder but was consistent with the presence of $[Ir(CO)(dppms)I_2(COMe)]$ having distorted octahedral geometry with CO *trans* to iodide and acetyl *trans* to S of the dppms chelate. By contrast, in situ high-pressure IR spectroscopy revealed no decay or shift of the ν(CO) absorption of **5b** over 3 h under the same conditions. The iridium methyl complexes **5a** and **5b** therefore display the same trend in reactivity as their rhodium analogues **2a** and **2b**. Evidence was obtained that carbonylation of **5b** could be induced at higher temperature, a product with ν(CO) absorptions at 2057 and 1649 cm^{-1} (CH_2Cl_2) being obtained after treatment of a solution of **5b** with 9 bar of CO in a Fisher Porter vessel at 120 °C for 3 h.

X-ray Crystallographic Studies. The X-ray crystal structure of the iridium methyl complex **5a** (Figure 3) displays a pseudo-octahedral geometry with the methyl group occupying a position *cis* to both P and S donor atoms of the dppms ligand. The carbonyl ligand is *trans* to S, as for the Ir(I) precursor. The five-membered chelate ring adopts an envelope conformation with the methylene carbon at its apex. This conformation places two of the dppms phenyl groups in pseudoaxial positions and creates a crowded "pocket" surrounding the methyl ligand. The other two phenyl groups are placed in pseudoequatorial positions, such that the iodide *trans* to methyl is in a much less crowded environment. The adoption of this conformation can be explained by the smaller cone angle of methyl (90°) compared with iodide (107°).[1] The closest nonbonded contact

value of A(2062)/A(1987) at 8 M MeI. This was then converted into a ratio of concentrations, [**2a**]/[**1a**], by dividing by 0.6 the ratio of extinction coefficients measured for the ν(CO) bands of the Ir analogues **5a** and **4a**.

(37) In our preliminary communication of these results (ref 16) the influence of isomeric forms of **2b** on the migratory insertion rate constant was neglected.

(38) Haynes, A.; Mann, B. E.; Gulliver, D. J.; Morris, G. E.; Maitlis, P. M. *J. Am. Chem. Soc.* **1991**, *113*, 8567.

(39) Atwood, J. D. In *Comprehensive Organometallic Chemistry II*; Abel, E. W., Stone, F. G. A., Wilkinson, G., Eds.; Pergamon: Oxford, 1995; Vol. 8, p 303.

(40) Pearson, J. M.; Haynes, A.; Morris, G. E.; Sunley, G. J.; Maitlis, P. M. *J. Chem. Soc., Chem. Commun.* **1995**, 1045.

(41) Calculated rate at 93 °C using the activation parameters $\Delta H^{\ddagger} = 33$ kJ mol^{-1} and $\Delta S^{\ddagger} = -197$ J mol^{-1} K^{-1} for carbonylation of $[Ir(CO)_2I_3Me]^-$ in 25% (v/v) MeOH−PhCl (ref 40) and dividing by 25 to compensate for the different MeOH concentrations.

Table 5. Distances and Angles between Pseudoaxial Phenyl Groups in Complexes of dppms, dppmo, and dppe

complex	geometry	r_{ipso}, Å	r_{cent}, Å	θ, deg	ref
[Rh(CO)(dppms)Cl]	sq pl	3.49	3.89	15	10
[Pd(dppms)I_2]	sq pl	3.43	3.78	9	42
[Pd(dppms)$_2$]$^{2+}$	sq pl	3.55	4.11	17	42
[Rh(CO)(dppmo)Cl]	sq pl	4.10	5.09	35	12
[Hg(dppms)I_2]	tet	3.67	4.03	19	43
[Rh(dppms)I_2(COMe)] (**3a**)	sq pyr	3.42	3.70	10	
[Rh(dppe)I_2(COMe)] (**3b**)	sq pyr	4.25	5.04	55	
[Ir(CO)(dppms)I_2Me] (**5a**)	oct	3.73	4.23	39	
[Ir(CO)(dppms)I_2Et] (**6**)	oct	4.13	4.91	45	
[{Ir(CO)(dppms)I_2Me}$_2$]$^{2+}$ (**7**)	oct	3.77	4.44	44	

between hydrogens of the phenyl and methyl groups (H5A and H2A) is ca. 1.9 Å, which is less than double the van der Waals radius of hydrogen. This steric interaction causes the methyl ligand to lean away from the phenyl group, giving a P−Ir−Me bond angle of 96°, which is the biggest deviation from regular octahedral geometry in the complex. By contrast the P−Ir−Me angles in **5b** are both close to 90°.[24] The crystal structures therefore suggest that steric interactions might play a role in accelerating migratory insertion in **2a** and **5a** compared to analogous dppe complexes.

It is informative to compare the structure of **5a** with complexes of dppms which have fewer than two "axial" ligands (where the equatorial plane is defined as that containing the metal atom and the two donor atoms of the bidentate ligand). The structure of [Rh(CO)(dppms)Cl] determined by Baker et al.[10] exhibits a ligand conformation where two axial phenyls block one face of the square planar complex. Again the five-membered chelate ring adopts an envelope structure, but in this case the sulfur-bound phosphorus is at the apex. Very similar dppms ligand conformations are displayed in the recently reported[42] square planar palladium(II) complexes [Pd(dppms)I_2] and [Pd(dppms)$_2$]$^{2+}$ and in the tetrahedral [Hg(dppms)I_2].[43]

A measure of the spatial arrangement of the axial phenyl groups is provided by the distances between the *ipso* carbons (r_{ipso}) or the ring centroids (r_{cent}) along with the angles between the phenyl planes (θ) given in Table 5. For the square planar dppms complexes θ is less than 20° with r_{ipso} = ca. 3.5 Å and r_{cent} = ca. 3.8 Å (except in the more crowded bischelate [Pd(dppms)$_2$]$^{2+}$). In [Hg(dppms)I_2] the phenyl rings move apart slightly to accommodate an iodide in the tetrahedral structure. An approximate parallel stacking arrangement (with θ = 10°) is maintained in the square pyramidal rhodium acetyl complex **3a** (Figure 1), with the axial phenyls flanking the vacant sixth coordination site, allowing the acetyl ligand to occupy the sterically less demanding axial site. The space-filling diagrams in Figure 8 show how θ widens to 39° to accommodate the methyl ligand in **5a**. This is achieved by a twist of the phenyl attached to the iridium-bound phosphorus.[44] An even more pronounced distortion is apparent for the ethyl analogue **6**, in which θ is 45°. The accommodation of the ethyl ligand in **6** forces significant rearrangement in the chelate ring, which has the Ir-bound phosphorus at the apex of the envelope, leading

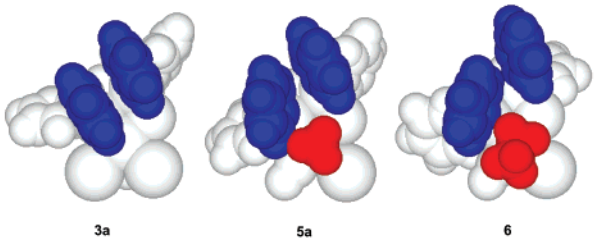

Figure 8. Space-filling models of the X-ray structures of complexes **3a**, **5a**, and **6**. Note the increasing separation and widening of the angle between the axial phenyl groups (shaded blue) caused by the introduction of methyl and ethyl ligands (shaded red) in **5a** and **6**, respectively.

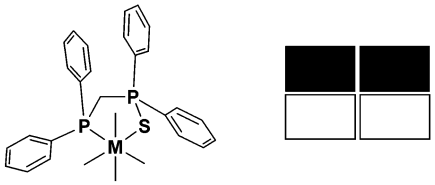

Figure 9. Ligand conformation and quadrant diagram for dppms complexes.

to reorientation of the equatorial phenyl groups. The structural rearrangements caused by axial methyl or ethyl ligands in **5a** and **6** are also evident from the larger values of r_{ipso} and r_{cent} for these complexes in Table 5.

A feature of all the structures containing the dppms ligand is the steric crowding of one axial coordination site due to the disposition of two of the phenyl groups. This steric environment can be expressed in terms of a quadrant diagram (Figure 9).[45] When the two phenyls flank a vacant site (e.g., in square planar or square pyramidal complexes), they can stack approximately parallel, whereas in an octahedral complex, an axial ligand is placed in the sterically crowded region, which disrupts the stacking. The conformation adopted by phenyl groups in dppe complexes is noticeably different from that described above for the dppms ligand. For example, the angle between the planes of the phenyl groups flanking the vacant coordination site in **3b** is 55°, compared with 10° in the dppms analogue **3a**. This suggests that there is much less preference for phenyl groups to stack parallel in the dppe system. A detailed analysis of structures of this type by Morton and Orpen[46] revealed that the five-membered M(dppe) chelate ring typically adopts a twist (C_2) rather than an envelope conformation, with a weak preference for the conformation of phenyl groups shown in Figure 10a, in which diagonal quadrants are more hindered. The X-ray structures of octahedral complexes **5b**[24] and [Ir(dppe)I_4]$^-$[47] display just such a conformation with little crowding of the axial methyl or iodide ligands.

Morton and Orpen also considered the M_2(μ-dppm) fragment and revealed a preferred conformation (Figure 10b) very similar to that observed for M(dppms).[46] It was concluded that the M_2(μ-dppm) ring is more rigid than the M(dppe) system and places greater constraints on the conformation of the phenyl groups. The M(dppms) chelate ring can be regarded as analogous to a dinuclear M_2(μ-dppm) system, with a sulfur replacing one of the metal atoms, so similar conformational preferences are to be expected. The driving force for adoption of the stacked

(42) Wong, T. Y. H.; Rettig, S. J.; James, B. R. *Inorg. Chem.* **1999**, *38*, 2143.
(43) Lobana, T. S.; Sandhu, M. K.; Liddell, M. J.; Tiekink, E. R. T. *J. Chem. Soc., Dalton Trans.* **1990**, 691.
(44) As judged by the M−P−C_{ipso}−C_{ortho} dihedral angles of 10.6° in **3a** and 42.8° in **5a**. The corresponding dihedral angle for the other axial phenyl, S−P−C_{ipso}−C_{orth}, is small (<1°) in both structures.
(45) Knowles, W. S. *Acc. Chem. Res.* **1983**, *16*, 106.
(46) Morton, D. A. V.; Orpen, A. G. *J. Chem. Soc., Dalton Trans.* **1992**, 641.
(47) Chan, Y. N. C.; Meyer, D.; Osborn, J. A. *J. Chem. Soc., Chem. Commun.* **1990**, 869.

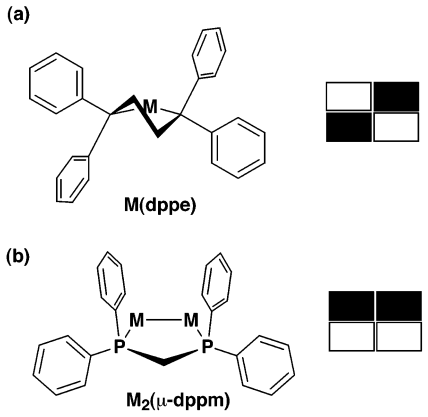

Figure 10. Conformations and quadrant diagrams for (a) M(dppe) and (b) $M_2(\mu$-dppm) complexes.

arrangement of axial phenyl groups in dppms complexes is primarily the envelope conformation of the chelate ring. An intriguing possibility is that attractive $\pi-\pi$ stacking interactions between the phenyls further stabilize this arrangement. Recent crystallographic and theoretical studies by Pregosin and coworkers[48] have concluded that attractive intramolecular $\pi-\pi$ stacking interactions between aromatic rings in coordinated ligands can result in significant structural distortion of square planar Pd(II) complexes. The distances between the phenyl rings for dppms complexes (Table 5) are close to the range (3.4−3.5 Å) for $\pi-\pi$ stacking in biological systems,[49] suggesting that such interactions might play a role in tuning organometallic reactivity.

On the basis of the structural analysis, we propose that migratory insertion in [M(CO)(dppms)I_2Me] (**2a**, M = Rh; **5a**, M = Ir) is accelerated (compared to that in the dppe analogues) by relief of the steric tension created by phenyl groups on the bidentate ligand. It is clear that the acetyl ligand of **3a** occupies a much less sterically demanding site than the methyl ligand in **5a**. If the steric crowding in **2a** (or **5a**) is partially removed in the transition state for methyl migration, then an acceleration will result (compared with complexes without similar steric strain). Although alternative ligand conformations are undoubtedly accessible in solution, the solid-state structures exhibit trends which are consistent with steric effects exerting an important influence on reactivity. A recent theoretical study on this system supports this argument (vide infra).[21]

Conformational analysis[46] suggested that the rigidity of the envelope structure (and constraints on the phenyl groups) in the $M_2(\mu$-dppm) fragment increases for longer M−M bonds. Conversely, a decrease in rigidity would be expected on shortening the M−M bond, an effect which can be mimicked in our system by replacing the dppms ligand with dppmo. Consistent with this, θ increases from 15° in [Rh(CO)(dppms)-Cl] (r_{Rh-S} = 2.403 Å)[10] to 35° in [Rh(CO)(dppmo)Cl] (r_{Rh-O} = 2.109 Å)[12] with corresponding increases in r_{ipso} and r_{cent} (Table 5). This reduction in steric crowding around one of the axial coordination sites when dppms is replaced by dppmo offers

Scheme 4. Mechanism for Reaction of **1a** with MeI

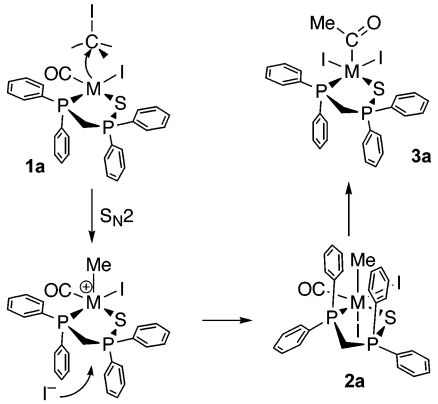

an explanation for the equilibrium between methyl and acetyl products **2c** and **3c** formed in the reaction of [Rh(CO)(dppmo)I] with MeI.

Reaction Mechanism for Oxidative Addition to 1a. In light of the above structural analysis we propose that the ligand conformation plays a key role in determining reactivity in the dppms system. The suggested sequence of reactions is shown in Scheme 4. Oxidative addition of methyl iodide to a square planar complex is generally believed to proceed in two steps: (i) nucleophilic attack by the metal center at carbon to displace I^- and (ii) coordination of I^- to the five-coordinate intermediate.[26,27] In the reaction of **1a** it is likely that the MeI molecule will approach the less-hindered face of the metal complex. The S_N2 step will generate an initial cationic intermediate, [Rh(CO)-(dppms)IMe]$^+$, in which the vacant coordination site is flanked by the axial phenyl groups. To complete the oxidative addition, iodide must coordinate to the vacant site, but since iodide has a larger cone angle than methyl, we propose that a change in ligand conformation accommodates the incoming iodide.[50] This generates an octahedral product in which the axial phenyl groups flank the methyl ligand, as found in the crystal structure of **5a**. Migratory CO insertion then proceeds with another change in ligand conformation to place the acetyl ligand in the less hindered axial coordination site, as in the crystal structure of **3a**. Steric congestion is therefore relieved by migratory insertion.

We attempted to model the product of the first (S_N2) step in Scheme 4 by treating **4a** with methyl triflate. The reaction gave a product with a ν(CO) band at 2058 cm^{-1} and analytical data consistent with a cationic Ir(III) complex with a triflate counterion, [Ir(CO)(dppms)IMe][OTf]. A solution of this product in CD_2Cl_2 shows four sets of signals in the ^{31}P NMR (see the Experimental Section), indicating the presence of isomers. Crystals grown from a CH_2Cl_2 solution were suitable for an X-ray diffraction study which revealed a centrosymmetric iodide-bridged dimer, [{Ir(CO)(dppms)(μ-I)Me}$_2$]$^{2+}$ (**7**) (Scheme 5 and Figure 11), together with two noncoordinated triflate anions and a molecule of solvent. Thus, the hoped-for five-coordinate intermediate actually dimerizes, at least in the solid state.

(48) Drago, D.; Pregosin, P. S.; Tschoerner, M.; Albinati, A. *J. Chem. Soc., Dalton Trans.* **1999**, 2279. Magistrato, A.; Merlin, M.; Pregosin, P. S.; Rothlisberger, U. *Organometallics* **2000**, *19*, 3591. Magistrato, A.; Pregosin, P. S.; Albinati, A.; Rothlisberger, U. *Organometallics* **2001**, *20*, 4178.

(49) Ranganathan, D.; Haridas, V.; Gilardi, R.; Karle, I. L. *J. Am. Chem. Soc.* **1998**, *120*, 10793. Hobza, P.; Kabelác, M.; Sponer, M.; Mejzlík, P.; Vondrásek, J. *J. Comput. Chem.* **1997**, *18*, 1136.

(50) The ^{1}H NMR spectra of **1a** and **4a** exhibit pseudotriplets indicating time-averaged equivalence of the two methylene protons of dppms due to rapid inversion of the chelate envelopes on the NMR time scale. The proposed changes in ligand conformation are therefore feasible. The ^{1}H NMR spectra of **3a**, **5a**, and **6** display pairs of signals with ddd patterns, due to inequivalent methylene protons with $^2J_{HH}$ and two $^2J_{HP}$ couplings. This inequivalence is conferred by unsymmetrical coordination in the two axial sites, and will be maintained even if the ligand conformation is fluxional.

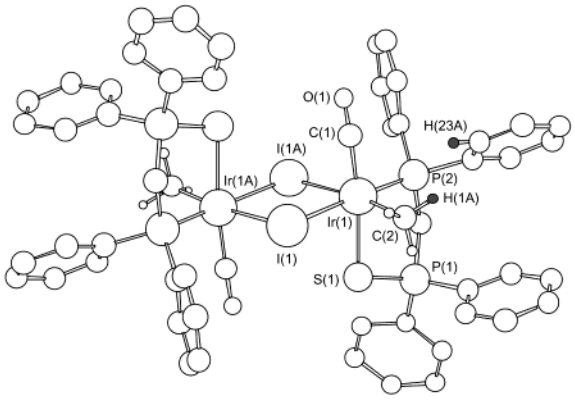

Figure 11. X-ray structure of $[Ir(CO)(dppms)(\mu\text{-}I)Me]_2OTf_2$ (**7**). Selected H atoms, triflate counterions, and a CH_2Cl_2 solvent molecule are omitted for clarity. Selected geometric data are given in Table 2.

Scheme 5. Addition of Methyl Triflate to **4a**

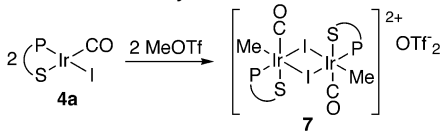

The coordination geometry around each Ir center in **7** is very similar to that in **5a**. The methyl ligand is again flanked by axial phenyl groups from the dppms ligand, which adopts an envelope conformation with the methylene carbon at its apex. The angle between the phenyl planes, θ, is 5° wider than in **5a**, and the methyl again leans away from the coordinated phosphorus, with the bond angle P(2)−Ir(1)−C(1) = 97°. Reaction of **7** with a stoichiometric amount of Bu_4NI in CH_2Cl_2 resulted in bridge cleavage to give **5a**, with IR and ^{31}P NMR spectra identical to those of a sample synthesized by the addition of MeI to **4a**. These results support the two-step mechanism for oxidative addition of MeI, but dimerization of the five-coordinate cation precluded an investigation of its ligand conformation.

A recent investigation[51] into the structure and reactivity of $[Rh(CO)\{\kappa^2\text{-}(P,S)\text{-}Fe(\eta^5\text{-}C_5Me_4P(S)Ph_2)(\eta^5\text{-}C_5Me_4PPh_2)\}Cl]$ (**8**) makes an interesting comparison to the dppms system. The

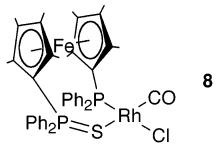

8

ν(CO) frequency of **8** (1987 cm^{-1}) is similar to that of the dppms analogue (1992 cm^{-1}), suggesting that the two P,S bidentate ligands have similar donor ability.[52] An X-ray crystal structure of **8** shows that the carbonyl ligand is coordinated *trans* to S as in **1a** and that one face of the square planar Rh(I) complex is effectively blocked by the ferrocene fragment. The reaction of **8** with MeI gave no rhodium(III) methyl or acetyl products, but instead resulted in halide metathesis to give the analogous iodide complex and MeCl. Further reaction with MeI resulted in dissociation of the bidentate ligand and quaternization of its PPh_2 group. These results were interpreted on the basis that the bulky ferrocene fragment prevents complete oxidative addition of MeI to give an octahedral methyl complex, and it would seem that steric effects in this system are more extreme than for the dppms ligand.

Relevance to Catalytic Methanol Carbonylation. To promote rhodium/iodide-catalyzed methanol carbonylation, ligands are sought which act as good electron donors, thus binding effectively to rhodium and increasing the nucleophilicity of the metal center toward MeI. Using the experimental activation parameters for oxidative addition of MeI to **1a** (Table 3), extrapolation to 185 °C gives a predicted rate constant of 1.25 (+0.8, −0.5) $dm^3\ mol^{-1}\ s^{-1}$ compared with a value of 2.16 $dm^3\ mol^{-1}\ s^{-1}$, calculated from the carbonylation rate reported by Baker et al. for a dppms-promoted Rh catalyst.[10] Thus, the model kinetic data fully support rate-determining oxidative addition of MeI to **1a** in the catalytic system.

Most phosphine ligands found to accelerate the oxidative addition step (e.g., PEt_3, dppe) tend to slow the subsequent migratory CO insertion step, for electronic reasons considered below. The dppms ligand is unusual in that it promotes both MeI oxidative addition and migratory insertion relative to the corresponding reactions in the catalytic cycle for $[Rh(CO)_2I_2]^-$. Extrapolation using the experimental activation parameters in Table 4 predicts a rate constant of ca. $2 \times 10^3\ s^{-1}$ for migratory insertion in **2a** at 185 °C, consistent with this step being fast relative to oxidative addition. Thus, while dppms fulfills the role of a good donor ligand, it also has the appropriate properties to encourage methyl migration.

A common problem associated with ligand-promoted methanol carbonylation processes is the long-term stability of the metal−ligand bonds. For example, the PEt_3-promoted system reported by Rankin et al. gave high catalytic activity for only 15 min (at 150 °C).[28] After this time, "normal" catalytic rates associated with the presence of the conventional $[Rh(CO)_2I_2]^-$ catalyst were observed, the phosphine ligand being lost from the metal coordination sphere as PEt_3Me^+, PEt_3H^+, and O=PEt_3. In the dppms-promoted system, the reported high catalytic rates (compared to those of $[Rh(CO)_2I_2]^-$) can be sustained for up to 1 h (at 185 °C). After more prolonged reaction times, activity drops and a Rh(dppm) complex can be isolated from the reaction mixture,[53] indicating catalyst deactivation resulting from extrusion of sulfur from the dppms ligand. GC analysis of the reactor headspace indicated the presence of H_2S.[54] The exact mechanism by which dppms ligand degradation occurs during catalysis is unclear, although dechelation of the sulfur arm of the chelate followed by reaction with water, acid, or H_2 (formed by the water gas shift reaction) are all feasible.[55] The in situ IR spectroscopic data (at 185 °C and 70 bar of CO) gave no evidence for detectable quantities of species with a monodentate dppms ligand, the only complex observed during the period of high catalytic activity being the chelate complex **1a**.

(51) Broussier, R.; Laly, M.; Perron, P.; Gautheron, B.; Nifant'ev, I. E.; Howard, J. A. K.; Kuz'mina, L. G.; Kalck, P. *J. Organomet. Chem.* **1999**, *587*, 104.
(52) Similarly the iodide M has ν(CO) 1981 cm^{-1} compared with 1987 cm^{-1} for **1a**.
(53) $^{31}P\{^1H\}$ NMR spectroscopic analysis of the residue recovered from catalytic reactions shows a doublet at δ −43.0 (J_{RhP} = 84 Hz) characteristic of a Rh(dppm) complex with equivalent P nuclei. In situ IR spectroscopy also indicates formation of some $[Rh(CO)_2I_2]^-$ after prolonged reaction.
(54) In a reaction which resembles the reverse of the dppms ligand degradation found here, $Pd_2(\mu\text{-dppm})$ complexes are reported to desulfurize H_2S, giving dppms as a byproduct. Wong, T. Y. H.; Barnabas, A. F.; Sallin, D.; James, B. R. *Inorg. Chem.* **1995**, *34*, 2278. See also ref 42.
(55) Reversible migration of alkyl groups from acetyl to sulfur (via intermediate rhodium alkyl species) has been reported in complexes of the type $[Rh(PPh_3)(L)(mnt)(COR)]$ (mnt = maleonitriledithiolate) (Cheng, C.-H.; Spivack, B. D.; Eisenberg, R. *J. Am. Chem. Soc.* **1977**, *99*, 3003. Cheng, C.-H.; Eisenberg, R. *Inorg. Chem.* **1979**, *18*, 2438).

This contrasts with the observations of Wegman et al., who found that a dicarbonyl, $[Rh(CO)_2I(dppeo)]$, with monodentate P-coordinated dppeo was the only species present during catalytic carbonylation reactions at 80 °C and ~3 bar of CO.[12] Thus, dppms shows much less propensity for hemilabile behavior than dppeo. This can be rationalized by the greater stability of five-membered compared with six-membered chelate rings, coupled with the stronger bonding of sulfur to a soft Rh(I) center. The dppeo ligand was found not to be an effective promoter at the higher temperature and pressure employed for the dppms system. It appears, therefore, that retention of the Rh(dppms) chelate structure is key to achieving high catalytic activity. This structure confers the appropriate electronic and steric environment to the Rh center for promotion of both MeI oxidative addition and CO insertion steps, as shown by our model studies under mild conditions.

Diphosphine ligands, while promoting oxidative addition to a degree similar to that of dppms, are not found to be as effective for catalytic methanol carbonylation. For example, dppe gave a catalytic rate an order of magnitude lower than that of $[Rh(CO)_2I_2]^-$, although some improvement over dppe was attained using unsymmetrical derivatives with fluorinated aryl groups, $Ph_2PCH_2CH_2PAr^F_2$.[15] In situ IR data reported for a catalytic reaction using the ligand with $Ar^F = C_6H_2F_3$-3,4,5 showed the absence of any terminal ν(CO) absorptions, suggesting that the catalyst resting state is not [Rh(CO)(L−L)I]. It is thought that acetyl complexes $[Rh(L-L)I_2(COMe)]$ are the resting states for these systems, the acetyl ν(CO) band being masked by the solvent.

Despite the low activity for acetic acid formation, diphosphines (e.g., dppp) have been shown to be effective for the rhodium/iodide-catalyzed *reductive* carbonylation of methanol.[14,18]

$$MeOH + CO + H_2 \rightarrow MeCHO + H_2O \qquad (7)$$

Kinetic studies showed the reaction to be first-order in $[Rh(dppp)I_2(COMe)]$ but zero-order in MeI, and it was proposed that reaction of $[Rh(dppp)I_2(COMe)]$ with H_2 determined both the rate and acetaldehyde selectivity. Consistent with this, extrapolation of our kinetic data for the dppe system to 140 °C predicts that neither oxidative addition nor migratory insertion should be rate-limiting for reductive carbonylation.[56]

Five-coordinate acetyl intermediates $[Rh(L-L)I_2(COMe)]$ are clearly important in these catalytic carbonylation reactions, and we find a significant difference in reactivity toward CO for L−L = dppms and dppe. Baker et al. reported that reaction of **3a** with 30 atm of CO gave two isomers of $[Rh(CO)(dppms)I_2(COMe)]$. We find that the same conversion is achieved by simply bubbling CO (1 atm) through a solution of **3a** in CH_2Cl_2 for 1 h, as judged by product terminal and acetyl ν(CO) bands at 2085 and 1685 cm^{-1}. On standing under CO (1 atm) for 24 h, the formation of an IR band at 1987 cm^{-1} indicated the regeneration of **1a** by reductive elimination of acetyl iodide. By contrast, similar treatment of **3b** did not give $[Rh(CO)(dppe)I_2(COMe)]$ or any sign of reductive elimination to regenerate **1b**. This concurs with the results of Moloy and Wegman,[14] who did not detect $[Rh(CO)(dppe)I_2(COMe)]$ and found that acetic acid could only be generated from **3b** at 140 °C under a pressure of CO. Thus, the dppms ligand also favors the reductive elimination step compared with diphosphine complexes.

Chart 1. Diphosphine Ligands for Catalytic CO/Alkene Copolymerization and Hydroformylation

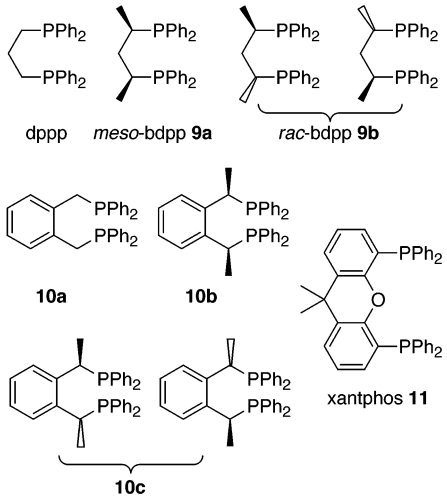

Relationship to Other Catalytic Reactions. It has long been appreciated that an orientation of phenyl groups which shields two *diagonal* quadrants is required for effective asymmetric hydrogenation catalysts.[45,57] However, there are other catalytic reactions where there may be a requirement for steric hindrance concentrated in two adjacent quadrants, as found in the dppms system. Recent studies of ligand effects on Pd-catalyzed CO/ethene copolymerization by Bianchini et al.[58] have shown that modification of the backbone of the conventional dppp ligand gives some noteworthy effects on catalytic behavior. For example, *meso*-bdpp (**9a**) (Chart 1) gave catalysts with higher activity than both dppp itself and *rac*-bdpp (**9b**). A similar activity trend was shown by Sesto and Consiglio[59] for CO/propene copolymerization. Even more dramatic effects on activity and regioregularity were achieved with the ligands **10a**−**c** for which the *meso* ligand **10b** again gave the most active and regioselective catalyst. These effects are clearly steric in origin, and Bianchini's interpretation stressed the importance of the spatial distribution of the phenyl groups, with the *meso* ligands creating a coordination sphere with steric crowding concentrated on one face of the Pd complex.

Earlier studies of CO/alkene copolymerization determined that, of the $R_2P(CH_2)_nPR_2$ series, the ligand of choice for high catalytic activity and a high molecular weight polymer was dppp (i.e., R = Ph and $n = 3$), the order of activity for the R = Ph ligands following the order $n = 3$ (dppp) > 2 (dppe) > 4 (dppb).[60] This trend was reproduced more recently by Koide et al., who introduced the concept of a *pocket angle* (or *interior ligand cone angle*) to quantify diphosphine ligand steric requirements, and suggested that dppp gave the optimum size

(56) The activation parameters in Tables 3 and 4 predict catalytic reductive carbonylation rates of ca. 15 or 200 mol dm^{-3} h^{-1} if, respectively, oxidative addition or migratory insertion is rate-limiting under the conditions in ref 14. The reported maximum catalytic rate is 6 mol dm^{-3} h^{-1}.

(57) Zhu, G.; Cao, P.; Jiang, D.; Zhang, X. *J. Am. Chem. Soc.* **1997**, *119*, 1799. Koenig, K. E.; Sabacky, M. J.; Bachman, G. L.; Christopfel, W. C.; Barnstorff, H. D.; Friedman, R. B.; Knowles, W. S.; Stults, B. R.; Vineyard, B. D.; Weinkauff, D. J. *Ann. N. Y. Acad. Sci.* **1980**, *333*, 16.
(58) Bianchini, C.; Lee, H. M.; Barbaro, P.; Meli, A.; Moneti, S.; Vizza, F. *New J. Chem.* **1999**, *23*, 929. Bianchini, C.; Lee, H. M.; Meli, A.; Moneti, S.; Vizza, F.; Fontani, M.; Zanello, P. *Macromolecules* **1999**, *30*, 44183.
(59) Sesto, B.; Consiglio, G. *J. Am. Chem. Soc.* **2001**, *123*, 4097.
(60) Drent, E.; Budzelaar, P. H. M. *Chem. Rev.* **1996**, *96*, 663. Drent, E.; van Broekhoven, J. A. M.; Doyle, M. J. *J. Organomet. Chem.* **1991**, *417*, 235.

and shape of the active site.[7] X-ray crystal structures of [Pd(dppe)Cl(CO^{t}Bu)] and [Pd(dppp)Cl(CO^{t}Bu)] showed that the dppp complex has adjacent hindered quadrants blocking one face of the coordination plane whereas steric hindrance in the dppe complex is more dispersed.[61]

Bidentate phosphine ligands are also commonly used in rhodium-catalyzed hydroformylation reactions. A wide range of ligands have been tested, with particular recent emphasis on the control of catalytic activity and product linear:branched (l:b) ratios by tuning the ligand bite angle.[5,6,62] There remains, however, considerable debate about the precise mechanism by which a change in ligand bite angle affects the catalytic properties. In the words of Casey et al.,[6] "The regioselectivity of hydroformylation is governed by a complex web of electronic and steric effects that have so far defied unraveling." A recent theoretical study of Rh hydroformylation catalysts containing xantphos (**11**) and related ligands concluded that "the leading role in determining the regioselectivity is played by the diphenylphosphino substituents" and that electronic (or "orbital") effects have little influence.[63] The calculated structures of [Rh(CO)(alkene)(diphosphine)H] in that study show that the nonbonding interactions of phenyl groups with coordinated ligands are crucial in controlling the product l:b ratio. Interestingly, the axial phenyl rings in [Rh(CO)(ethene)(benzoxantphos)H] were found to be virtually parallel when they flanked an axial hydride ligand, but when the larger CO was placed in this site, the phenyls moved apart (Figure 2 in ref 62), closely resembling the ligand distortions we observe (Figure 8), in which alkyl ligands force the dppms phenyls to move apart. While a number of effects (e.g., bite angle, donor strength, hemilability) are at work in determining the behavior of different hydroformylation catalysts, the steric influence of phosphine ligand substituents is clearly an important contributor. The "embracing" effect of phenyl rings has also been invoked to explain the effect of diphosphine bite angle on the ratio of *syn* and *anti* isomers in [Pd(1-methallyl)(diphosphine)]$^+$ complexes and thus the influence on the regiochemistry of allylic alkylation reactions.[64] The steric effects we have identified are therefore closely related to those believed to influence a range of catalytic processes.

Electronic Considerations. The structural studies described above provide one explanation for the observed ligand effects, involving steric (nonbonding) interactions. The contribution of electronic (through-bond) interactions must also be considered, since the IR data show clearly that dppms and dppe differ in their donor properties. Good donor ligands, while promoting oxidative addition, normally retard CO insertion, as for the dppe PEt_3[28] systems. One explanation for this is the formation of stronger metal−alkyl bonds by the more nucleophilic precursors. Another consideration is that higher electron density on the metal leads to stronger M(d) → CO(π*) back-bonding, which is expected to inhibit CO insertion by decreasing the electrophilicity of the carbonyl carbon.[65] Indeed, migratory insertion is often found to be enhanced by coordination of π-acceptor ligands.[66] On the basis of these arguments, the rapid migratory insertions observed for **2a** and **2c** are surprising, since the observed ν(CO) frequencies suggest greater back-donation from Rh to CO in **2a** (2062 cm^{-1}) and **2c** (2057 cm^{-1}) compared with **2b** (2076 cm^{-1}). Thus, the S and O donor atoms appear to exert a π-pushing effect which raises the Rh d orbital energies and enhances back-donation to CO. This is expected to inhibit rather than promote migratory CO insertion.

Most of the experimental evidence suggests the chelate rings in these systems are relatively robust, at least under the mild conditions of the model studies. However, the behavior of complexes **1a**−**c** in the presence of excess iodide anion indicated that hemilabile behavior might be possible. If one arm of the chelate ligand were to dissociate (most probably the S or O arm of dppms or dppmo, respectively[67]), the consequent reduction in electron density on the Rh center and decrease in Rh−CO back-donation would be expected to favor methyl migration (although an unstable 14-electron acetyl species would be the initial product before chelate ring closure). We are doubtful that chelate ring opening occurs under mild conditions (where rapid migratory insertion still occurs for **2a** and **2c**), but under the more forcing conditions of the catalytic reactions, this mechanism cannot be excluded.

Ab Initio Calculations. Since publication of our preliminary communication,[16] Cavallo and Sola have applied density functional theory (DFT) to some of the same systems.[21] In addition to simple models, in which hydrogens replaced phenyls, their study reported calculations with the full-size ligands, using both hybrid QM/MM and pure QM methods. They concluded that steric crowding introduced by ligand phenyl substituents results in less exothermic oxidative addition, but a lower activation barrier for migratory CO insertion, in agreement with the conclusions of our experimental study.[68] The experimental migration insertion barrier for **2a** was reproduced extremely well by the calculations, whereas that for **2b** was underestimated. The theoretical results support the experimental observation that migratory insertion is much faster for **2a**, and do not require dissociation of the S donor arm of dppms to achieve the lower activation barrier. Another feature of the DFT study is that the CO insertion barrier was predicted to be lower for the P,S chelate complex even in the simple models where hydrogens replaced phenyls. This suggested to us that there might be an electronic contribution to the difference in reactivity, in addition to the steric effects described above. Independently of the study by Cavallo and Sola, we have carried out ab initio MP2 calculations

(61) Dppms has recently been found to give Pd catalysts with moderate activity for CO/ethene copolymerization, whereas catalysts using $Ph_2PCH_2CH_2P(S)Ph_2$ (which forms a six- rather than five-membered chelate ring) give ca. 50% lower activity (Suranna, G. P.; Mastrorilli, P.; Nobile, C. F.; Keim, W. *Inorg. Chim. Acta* **2000**, *305*, 151).

(62) Kamer, P. C. J.; Reek, J. N. H.; van Leeuwen, P. W. N. M. *CHEMTECH* **1998**, 27. van der Veen, L. A.; Boele, M. D. K.; Bregman, F. R.; Kamer, P. C. J.; van Leeuwen, P. W. N. M.; Goubitz, K.; Fraanje, J.; Schenk, H.; Bo, C. *J. Am. Chem. Soc.* **1998**, *120*, 11616. Casey, C. P.; Paulsen, E. L.; Beuttenmueller, E. W.; Proft, B. R.; Matter, B. A.; Powell, D. R. *J. Am. Chem. Soc.* **1999**, *121*, 63.

(63) Carbo, J. J.; Maseras, F.; Bo, C.; van Leeuwen, P. W. N. M. *J. Am. Chem. Soc.* **2001**, *123*, 7630.

(64) van Harren, R. J.; Oevering, H.; Coussens, B. B.; van Strijdonck, G. P. F.; Reek, J. N. H.; Kamer, P. C. J.; van Leeuwen, P. W. N. M. *Eur. J. Inorg. Chem.* **1999**, 1237.

(65) Margl, P.; Ziegler, T.; Blöchl, P. E. *J. Am. Chem. Soc.* **1996**, *118*, 5412.

(66) Cardaci, G.; Reichenbach, G.; Bellachioma, B.; Wassink, B.; Baird, M. C. *Organometallics* **1988**, *7*, 2475. Wright, S. C.; Baird, M. C. *J. Am. Chem. Soc.* **1985**, *107*, 6899. Bellachioma, B.; Cardaci, G.; Macchioni, A.; Reichenbach, G.; Foresti, E.; Sabatino, P. *J. Organomet. Chem.* **1997**, *531*, 227. Kubota, M.; McClesky, T. M.; Hayashi, R. K.; Webb, C. G. *J. Am. Chem. Soc.* **1987**, *109*, 7569. Ghaffar, T.; Adams, H.; Maitlis, P. M.; Sunley, G. J.; Baker, M. J.; Haynes, A. *Chem. Commun.* **1998**, 1023.

(67) Ab initio calculations indicate that displacement of the S or O donor by CO in $[Rh(CO)(H_2PCH_2P(X)H_2)I]$ is more favorable by 11 kJ mol^{-1} (X = S) or 12 kJ mol^{-1} (X = O) than displacement of a PH_2 donor in $[Rh(CO)(H_2PCH_2CH_2PH_2)I]$.

(68) The dppms ligand conformations in the DFT-calculated structures of **1a** and **2a** in ref 21 differ somewhat from the conformations found in related X-ray structures. In particular, the parallel stacked arrangement of axial phenyls, found consistently by experiment, is not well reproduced.

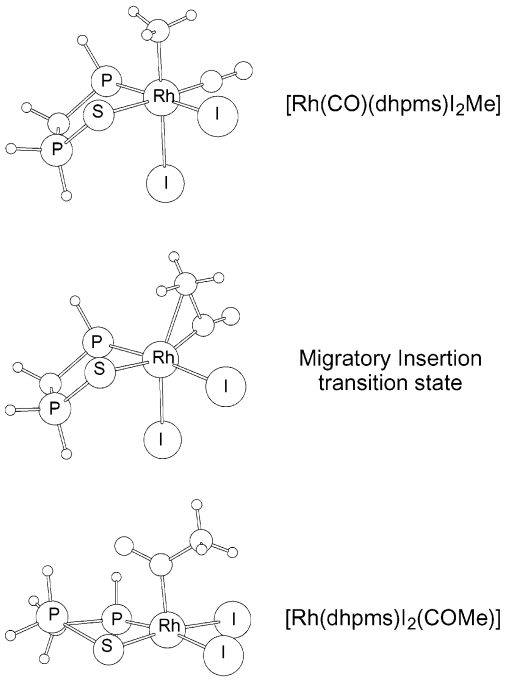

Figure 12. Stationary points on the reaction coordinate for migratory insertion in [Rh(CO)(dhpms)I_2Me].

Table 6. Calculated Activation Energies $\Delta E^{\ddagger}$ and Reaction Energies ΔE for Migratory Insertion in [Rh(CO)(L−L)I_2Me] or [Rh(CO)$(PH_3)_2I_2$Me]

ligand	geometry	method	$\Delta E^{\ddagger}$, kJ mol^{-1}	ΔE, kJ mol^{-1}	$\Delta E^{\ddagger}_{orb}$,[a] kJ mol^{-1}
dhpms	CO *trans* to S	MP2	99	12	58
dhpms	CO *trans* to P	MP2	110	20	106
dhpms	CO *trans* to S	DFT[21]	74	−36	
dppms	CO *trans* to S	DFT[21]	56	−56	
dhpmo	CO *trans* to O	MP2	104	42	98
dhpe	CO *trans* to P	MP2	116	34	117
dhpe	CO *trans* to P	DFT[21]	82	−40	
dppe	CO *trans* to P	DFT[21]	61	−57	
$(PH_3)_2$	CO *trans* to I	MP2	102	38	85
$(PH_3)_2$	CO *trans* to I	DFT[21]	68	−38	
$(PEt_3)_2$	CO *trans* to I	DFT[21]	78	−12	

[a] $\Delta E^{\ddagger}_{orb}$ is the difference in orbital energies of orbitals A and B as defined in the text and Figure 13.

on the simple model systems [i.e., $H_2PCH_2P(S)H_2$ (dhpms), $H_2PCH_2CH_2PH_2$ (dhpe), $H_2PCH_2P(O)H_2$ (dhpmo), and PH_3].

The optimized structures of stationary points for migratory insertion in [Rh(CO)(dhpms)I_2Me] are illustrated in Figure 12. In each case, the reaction proceeds via a transition state in which the methyl ligand has moved toward the carbonyl carbon, accompanied by some reduction of the Rh−C−O bond angle. The five-coordinate acetyl products all optimized with approximate square pyramidal geometry. While the absolute values of activation and reaction energies given by our calculations differ somewhat from the DFT results (Table 6), the trends are similar. We find the migratory CO insertion barrier to be 17 kJ mol^{-1} lower for [Rh(CO)(dhpms)I_2Me] than for [Rh(CO)(dhpe)I_2Me] (the DFT value is 8 kJ mol^{-1}). The barrier for [Rh(CO)(dhpmo)I_2Me] is marginally higher than for [Rh(CO)(dhpms)I_2Me]. For an isomer of [Rh(CO)(dhpms)I_2Me] with CO *trans* to P, the migration barrier is raised by 11 kJ mol^{-1}.

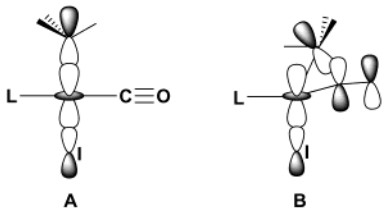

Figure 13. Important orbital interactions for migratory CO insertion.

For [Rh(CO)$(PH_3)_2I_2$Me], with CO *trans* to I, the migration barrier is similar those for the dhpms and dhpmo complexes.

These theoretical results suggest that the nature of the donor atom *trans* to CO has an influence on the migratory insertion barrier, but in the sense opposite to that predicted on the basis of simple arguments involving the strength of back-bonding. Cavallo and Sola did not offer any rationalization for this effect, which is also apparent in the results of their calculations. The orbital interactions important for the migratory insertion process have been identified previously,[65] as illustrated in Figure 13. In the octahedral methyl complex the Rh−CH_3 bond is formed by overlap of the Rh d_{z^2} orbital with a σ-donor orbital from the methyl group. This orbital also mixes with a p orbital on the iodine *trans* to methyl to give some Rh−I bonding character (A). In the transition state for methyl migration, this orbital is destabilized due to elongation of the breaking Rh−C bond and redirection of the local C_3 axis of the methyl group toward the carbonyl carbon (B). This destabilization is the greatest of any orbital involved in the migratory insertion and is therefore expected to be a major contributor to the activation barrier. The destabilization can be partially relieved by interaction with a CO π^* orbital, to initiate C−C bond formation. The calculated differences in orbital energies ($\Delta E^{\ddagger}_{orb} = E_B - E_A$) for the different ligand systems (Table 6) show the smallest destabilization for dhpms (with CO *trans* to S), and substantially larger destabilizations for dhpe and the dhpms isomer with CO *trans* to P. $\Delta E^{\ddagger}_{orb}$ takes intermediate values for the $(PH_3)_2$ complex (where CO is *trans* to I) and the dhpmo complex.

Inspection of the orbitals concerned in the dhpms system (Figure 14) reveals substantial mixing of transition-state orbital B with a sulfur p orbital, corresponding to significant Rh−S σ-bonding character, as well as Rh−Me and C(Me)−C(carbonyl) bonding. Mixing of this sort is not found for the corresponding orbital in the dhpe or dhpmo systems or when CO is *trans* to P in the dhpms system. It appears that a sulfur *trans* to CO can stabilize the migratory insertion transition state via this type of orbital interaction. The magnitude of this effect in the real system can only be speculated from the computational studies, and it is likely that the large difference in reactivity of the dppms and dppe systems results from a combination of steric and electronic factors. The noteworthy and surprising feature of the theoretical results is that an electronic effect reinforces the steric effect of the dppms ligand to promote migratory insertion, whereas simple bonding arguments predicted that electronic effects should operate in the opposite sense.

Conclusions

Our detailed mechanistic and kinetic study of the reactions of [M(CO)(L−L)I] with MeI has yielded considerable information regarding steric and electronic effects on oxidative addition

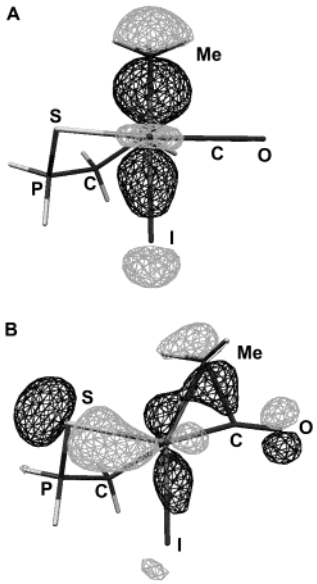

Figure 14. Important molecular orbitals A (reactant) and B (transition state) for migratory insertion in [Rh(CO)(dhpms)I_2Me]. The molecules are viewed along the equatorial I−Rh−P axis. Note the Rh−S bonding component which stabilizes the transition-state orbital B.

and migratory insertion. All the chelate ligands employed accelerate oxidative addition due to their good electron donor properties, but the promotion of migratory insertion by dppms was less expected. The promotion of *both* fundamental steps by the dppms ligand is unusual, and our investigations suggest that steric and electronic effects each contribute. X-ray crystal structures for several Rh and Ir complexes show that the conformation adopted by the dppms ligand creates steric congestion around one of the axial coordination sites, favoring the decrease in coordination number which accompanies methyl migration. This proposal is supported by recent DFT calculations. Our own ab initio calculations on model systems suggest that the placement of a sulfur donor ligand *trans* to CO also promotes migratory insertion, via an orbital interaction not obvious from simple bonding arguments. While hemilability of the chelate ligands is possible (and probably plays a role in catalyst deactivation), the model experimental and theoretical studies are consistent with intact chelate complexes giving rise to the high catalytic activity of the (dppms)Rh system.

Our results explain the high activity of dppms/Rh/iodide-catalyzed methanol carbonylation and also add quantitative understanding of the reaction steps in the reductive carbonylation reactions studied by Wegman and Moloy. They also have implications for the behavior of other catalytic systems, notably CO/alkene copolymerization and alkene hydrofomylation, where the influence of chelating diphosphine ligands is crucial. The "embracing" effect of the ligand phenyl groups of dppms models the steric effects of certain diphosphines (e.g., xantphos) used in hydroformylation, and suggests a mechanism by which the ligand bite angle can influence the behavior of the active site. Although similar interpretations have been given to explain catalytic behavior in various systems, quantitative reactivity data for individual reactions from a catalytic cycle, as we report here, are much more scarce.

Experimental Section

Materials. All solvents used for synthesis or kinetic experiments were distilled and degassed prior to use following literature procedures.[69] Synthetic procedures were carried out utilizing standard Schlenk techniques. Nitrogen and carbon monoxide were dried through a short (20 × 3 cm diameter) column of molecular sieves (4 Å) which was regularly regenerated. Carbon monoxide was also passed through a short column of activated charcoal to remove any iron pentacarbonyl impurity.[70] The ligand dppe was purchased from Aldrich and used without any further purification. The ligands dppms[71] and dppmo[72] and the complexes $[Rh(CO)_2Cl]_2$,[73] $[Rh(CO)_2I]_2$,[26] and $Bu_4N[Ir(CO)_2I_2]$[74] were synthesized according to literature procedures. Methyl iodide (Aldrich) was distilled over calcium hydride and stored in foil-wrapped Schlenk tubes under nitrogen and over mercury to prevent formation of I_2.

Instrumentation. FTIR spectra were measured using a Mattson Genesis Series spectrometer, controlled by WINFIRST software running on a Viglen 486 PC. High-pressure/high-temperature IR spectra were recorded on a Perkin-Elmer 1710 Fourier transform spectrometer using a SpectraTech cylindrical internal reflectance (CIR) cell (vide infra). $^{31}P\{^1H\}$ and ^1H NMR spectra were obtained using a Bruker AC250 spectrometer fitted with a Bruker B-ACS60 automatic sample changer operating in pulse Fourier transform mode, using the solvent as reference. Elemental analyses were performed using a Perkin-Elmer 2400 elemental analyzer.

Synthesis of Rhodium Complexes. (a) [Rh(CO)(dppms)I] (1a). $[Rh(CO)_2I]_2$ (100 mg, 0.17 mmol) was placed in a 50 cm^3 round-bottomed flask, and dissolved in CH_2Cl_2 (5 cm^3) to which a CH_2Cl_2 solution of dppms (0.23 g in 5 cm^3) was added. After 20 min, the volume of the solvent was reduced and diethyl ether was slowly added. The yellow precipitate obtained was filtered on a sinter, washed with ether, and air-dried. The solution was recovered, concentrated, and then left at −10 °C for 24 h to give a second crop of product. Yield: 219 mg (91%). Anal. Calcd for ($C_{26}H_{22}IOP_2RhS$): C, 46.5; H, 3.3; I, 19.1. Found: C, 46.3; H, 3.3; I, 18.8. IR (CH_2Cl_2): ν(CO)/cm^{-1} 1987. ^1H NMR (CD_2Cl_2): δ 8.10−6.85 (m, 20H, arom), 3.80 (pst, 2H, PCH_2P, $^2J_{HP}$ = 10 Hz). $^{31}P\{^1H\}$ NMR (CD_2Cl_2): δ 61.9 (dd, *P*═S, $^2J_{RhP}$ = 1 Hz), 51.3 (dd, Rh*P*, $^1J_{RhP}$ = 163 Hz, $^2J_{PP}$ = 60 Hz).

(b) [Rh(CO)(dppe)I] (1b). To a solution of $[Rh(CO)_2I]_2$ (50 mg, 0.10 mmol) in toluene (10 cm^3) was added a solution of dppe (100 mg, 0.25 mmol) in toluene (10 cm^3), dropwise. After 1 h, the product was obtained as a bright yellow precipitate, filtered, washed with ethanol and ether, and then air-dried. The solution was recovered, concentrated, and then left at −10 °C for 24 h. Yield: 70 mg (70%). Anal. Calcd for ($C_{27}H_{24}IOP_2Rh$): C, 49.4; H, 3.7; I, 19.3. Found: C, 49.0; H, 3.6; I, 19.6. IR (CH_2Cl_2): ν(CO)/cm^{-1} 2011. ^1H NMR (CD_2Cl_2): δ 8.10−7.15 (m, 20H, arom), 3.70−3.55 (m, 4H, PCH_2CH_2P). $^{31}P\{^1H\}$ NMR (CD_2Cl_2): δ 70.7 (dd, Rh*P trans* to I, $^1J_{RhP}$ = 161 Hz), 53.1 (dd, Rh*P trans* to CO, $^1J_{RhP}$ = 123 Hz, $^2J_{PP}$ = 32 Hz).

(c) [Rh(CO)(dppmo)I] (1c). $[Rh(CO)_2I]_2$ (57 mg, 0.1 mmol) was dissolved in a mixture of CH_2Cl_2 (2 cm^3) and toluene (5 cm^3). A solution of dppmo (40 mg, 0.2 mmol) in toluene (5 cm^3) was then added dropwise. After 30 min, the product was recovered by filtration as a yellow precipitate, washed with ether, and dried under vacuum. Yield: 55 mg (84%). Anal. Calcd for ($C_{26}H_{22}I_2O_2P_2Rh$): C, 47.5; H, 3.3; I, 19.3. Found: C, 47.7; H, 3.4; I, 18.9. IR (CH_2Cl_2): ν(CO)/cm^{-1} 1983. ^1H NMR (CD_2Cl_2): δ 7.75−7.20 (m, 20H, arom), 3.35 (pst, 2H, PCH_2P,

(69) Perrin, D. D.; Armerego, W. L. F.; Perrin, D. R. *Purification of Laboratory Chemicals*, 3rd ed.; Pergamon Press: Oxford, 1988.
(70) Haynes, A.; Ellis, P. R.; Byers, P. K.; Maitlis, P. M. *Chem. Br.* **1992**, *28*, 517.
(71) Grim, S. O.; Mitchell, J. D. *Synth. React. Inorg. Met.-Org. Chem.* **1974**, *4*, 221.
(72) Grim, S. O.; Satek, L. C.; Tolman, C. A.; Jesson, J. P. *Inorg. Chem.* **1975**, *14*, 656.
(73) McCleverty, J.; Wilkinson, G. *Inorg. Synth.* **1966**, *8*, 214.
(74) Forster, D. *Inorg. Nucl. Chem. Lett.* **1969**, *5*, 433.

$^2J_{HP}$ = 13 Hz). $^{31}P\{^1H\}$ NMR (CD_2Cl_2): δ 63.1 (dd, *P*═O, $^2J_{RhP}$ = 4 Hz), 41.9 (dd, Rh*P*, $^1J_{RhP}$ = 166 Hz, $^2J_{PP}$ = 33 Hz).

(d) [Rh(dppms)I$_2$(COMe)] (3a). 1a (50 mg) was dissolved in 10 cm^3 of CH_2Cl_2 under nitrogen. Methyl iodide (0.5 cm^3, excess) was added, and the solution was stirred at room temperature for 90 min and then concentrated in vacuo until cloudiness was observed. The product was precipitated as an orange powder by addition of diethyl ether after cooling to −10 °C, and recrystallized from CH_2Cl_2. Yield: 45 mg (75%). Anal. Calcd for ($C_{27}H_{25}I_2OP_2RhS$): C, 39.7; H, 3.1; I, 31.1. Found: C, 39.2; H, 2.9; I, 31.4. IR (CH_2Cl_2): ν(CO)/cm^{-1} 1701. ^1H NMR (CD_2Cl_2): δ 7.80−6.90 (m, 20H, arom), 4.88 (ddd, 1H, PC*H*H′P′, $^2J_{HP}$ = 8 Hz, $^2J_{HP'}$ = 4 Hz), 3.58 (ddd, 1H, PCH*H*′P′, $^2J_{H'P}$ = 5 Hz, $^2J_{H'P'}$ = 2 Hz, $^2J_{HH'}$ = 13 Hz), 3.16 (s, 3H, COCH_3). $^{31}P\{^1H\}$ NMR (CD_2Cl_2): δ 58.2 (dd, *P*═S, $^2J_{RhP}$ = 3 Hz), 55.1 (dd, Rh*P*, $^1J_{RhP}$ = 137 Hz, $^2J_{PP}$ = 46 Hz). A crystal suitable for an X-ray diffraction study was obtained by recrystallization from CH_2Cl_2.

(e) [Rh(dppe)I$_2$(COMe)] (3b). 1b (50 mg) was dissolved in 10 cm^3 of CH_2Cl_2 under nitrogen, then methyl iodide (0.5 cm^3, excess) was added, and the mixture was stirred at room temperature for 3 h. The solution was concentrated in vacuo until cloudiness was observed. The product was obtained as a yellow precipitate after addition of diethyl ether and cooling at −10 °C for 24 h. Yield: 42 mg (70%). Anal. Calcd for ($C_{28}H_{27}I_2OP_2Rh$): C, 42.1; H, 3.4; I, 31.8. Found: C, 41.9; H, 3.3; I, 32.0. IR (CH_2Cl_2): ν(CO)/cm^{-1} 1711. ^1H NMR (CD_2Cl_2): δ 7.82−7.73 and 7.52−7.23 (m, 20H, arom), 3.17−2.96 2.28−2.07 (m, 4H, PCH_2CH_2P), 2.65 (s, 3H, COCH_3). $^{31}P\{^1H\}$ NMR (CD_2Cl_2): δ 70.5 (d, $^1J_{RhP}$ = 139 Hz). Single crystals suitable for X-ray diffraction (vide infra) were obtained by recrystallization from CH_2Cl_2/diethyl ether.

Synthesis of Iridium Complexes. (a) [Ir(CO)(dppms)I] (4a). A solution of $Bu_4N[Ir(CO)_2I_2]$ (472 mg, 0.63 mmol) in toluene (10 cm^3) was added slowly to a solution of dppms (264 mg, 0.63 mmol) in a mixture of toluene (10 cm^3) and CH_2Cl_2 (5 cm^3) under N_2, and the resulting solution was stirred at room temperature for 1 h. The product was recovered as a yellow precipitate, filtered, washed with a mixture of EtOH/^{i}PrOH (1:2) followed by diethyl ether and hexane, and dried in vacuo. Yield: 390 mg (81%). Anal. Calcd for ($C_{26}H_{22}IIrOP_2S$): C, 40.9; H, 2.9; I, 16.6. Found: C, 40.6; H, 2.9; I, 16.9. IR (CH_2Cl_2): ν(CO)/cm^{-1} 1972. ^1H NMR (CD_2Cl_2) δ 7.70−7.10 (m, 20H, arom), δ 3.75 (pst, 2H, PCH_2P, $^2J_{HP}$ = 10 Hz). $^{31}P\{^1H\}$ NMR (CD_2Cl_2): δ 66.3 (d, *P*═S) 25.8 (d, Ir*P*, $^2J_{PP}$ = 54 Hz).

(b) [Ir(CO)(dppe)I] (4b). This synthesis followed the method of Fisher and Eisenberg.[17] $Bu_4N[Ir(CO)_2I_2]$ (400 mg, 0.5 mmol) was dissolved in THF (10 cm^3) and the resulting solution slowly added to a solution of dppe (200 mg, 0.5 mmol) in THF (15 cm^3) under N_2. The solution was stirred at moderate reflux for 1 h and then allowed to cool to room temperature. Ethanol (18 cm^3) was added, and a vigorous stream of N_2 was bubbled through the solution until an orange precipitate was obtained. The product was filtered and dried under vacuum. Yield: 280 mg (75%). Anal. Calcd for ($C_{27}H_{24}IIrOP_2$): C, 43.5; H, 3.2; I, 17.0. Found: C, 43.3; H, 3.4; I, 17.0. IR (CH_2Cl_2): ν(CO)/cm^{-1} 1994. ^1H NMR (CD_2Cl_2): δ 8.00−7.10 (m, 20H, arom), 2.45−2.04 (m, 4H, PCH_2CH_2P). ^{31}P NMR (CD_2Cl_2): δ 49.6 (d), 46.0 (d, $^2J_{PP}$ = 14 Hz).

(c) [Ir(CO)(dppms)I$_2$Me] (5a). 4a (390 mg, 0.51 mmol) was dissolved in CH_2Cl_2 (20 cm^3) and the solution stirred under N_2. Methyl iodide (0.5 cm^3, excess) was added, and the solution was stirred for 30 min. Diethyl ether was added until cloudiness appeared, and the flask was left at −10 °C for 24 h. The product was recovered as a cream-white precipitate, and recrystallized as yellow blocks from CH_2Cl_2. Yield: 336 mg (80%). Anal. Calcd for ($C_{27}H_{25}I_2IrOP_2S$): C, 35.8; H, 2.8; I, 28.0. Found: C, 35.4; H, 2.7; I, 28.3. IR (CH_2Cl_2): ν(CO)/cm^{-1} 2041. ^1H NMR (CD_2Cl_2): δ 7.95−6.71 (m, arom), 4.90 (ddd, PC*H*H′P′, major isomer, $^2J_{HH'}$ = 15 Hz, $^2J_{HP}$ = 5 Hz, $^2J_{HP'}$ = 2 Hz), 4.27 (ddd, PCH*H*′P′, major isomer, $^2J_{HH'}$ = 15 Hz, $^3J_{H'P}$ = 5 Hz, $^3J_{H'P'}$ = 3 Hz), 1.64 (d, IrCH_3, minor isomer), 1.25 (d, IrCH_3, major isomer) (both J_{HP} = 4 Hz). $^{31}P\{^1H\}$ NMR (CD_2Cl_2): δ 65.0 (d, P═*S*), 18.7 (d, Ir*P*, $^2J_{PP}$ = 36 Hz (major isomer)), 56.4 (d, P═*S*), 3.7 (d, Ir*P*, $^2J_{PP}$ = 23 Hz (minor isomer)). The two isomers identified by NMR spectroscopy were present in a ratio of ca. 3:1. An X-ray crystal structure of the major isomer was obtained (vide infra).

(d) [Ir(CO)(dppe)I$_2$Me] (5b). 4b (230 mg, 0.31 mmol) was dissolved in CH_2Cl_2 (20 cm^3) and stirred under N_2. Methyl iodide (0.5 cm^3, excess) was added, and the solution was stirred for 60 min. After the solvent had been reduced by half, hexane (10 cm^3) was added and the flask was cooled at −10 °C for 24 h. The product was recovered as a cream-white precipitate. Yield: 220 mg (81%). Anal. Calcd for ($C_{28}H_{27}I_2IrOP_2$): C, 37.9; H, 3.0; I, 28.6. Found: C, 37.7; H, 3.1; I, 28.5. IR (CH_2Cl_2): ν(CO)/cm^{-1} 2056. ^1H NMR (CD_2Cl_2): δ 8.01−7.58 (m, 20H arom), 3.07 (m, 4H, PCH_2CH_2P), 0.47 (dd, 3H, IrCH_3, $^3J_{HP}$ = 8, 5 Hz). ^{31}P NMR (CD_2Cl_2): δ 24.5 (d), −3.0 (d, $^2J_{PP}$ = 5 Hz). Spectroscopic data are in agreement with published data.[25]

(e) [Ir(CO)(dppms)I$_2$Et] (6). To **4b** (50 mg, 0.07 mmol) was added EtI (0.5 cm^3, excess) in CH_2Cl_2 (10 cm^3), and the solution was stirred for 24 h at room temperature. After reducing the solvent by half in vacuo, diethyl ether was added to give an orange precipitate which was recovered after cooling for 24 h at −10 °C and recrystallized from CH_2Cl_2. Yield: 34 mg (57%). Anal. Calcd for ($C_{28}H_{27}I_2IrOP_2S$): C, 36.6; H, 3.0; I, 27.6. Found: C, 36.2; H, 2.8; I, 28.1. IR (CH_2Cl_2): ν(CO)/cm^{-1} 2036. ^1H NMR (CD_2Cl_2): δ 8.05−6.93 (m, arom), 4.35 (ddd, PC*H*H′P′, major isomer, $^2J_{HH'}$ = 15 Hz, $^2J_{HP}$ = 11 Hz, $^2J_{HP'}$ = 4 Hz), 4.08 (ddd, PCH*H*′P′, major isomer, $^2J_{HH'}$ = 15 Hz, $^2J_{H'P}$ = 11 Hz, $^2J_{H'P'}$ = 5 Hz), 3.42 (q, IrCH_2CH$_3$, major isomer), 1.13 (t, IrCH$_2$CH_3, major isomer, $^3J_{HH}$ = 7 Hz). $^{31}P\{^1H\}$ NMR (CD_2Cl_2): δ 65.2 (d, P═*S*), 19.2 (d, Ir*P*, $^2J_{PP}$ = 36 Hz (major isomer)), 55.1 (d, P═*S*), 3.3 (d, Ir*P*, $^2J_{PP}$ = 25 Hz (minor isomer)). The two isomers identified by NMR spectroscopy were present in a ratio of ca. 3:1. An X-ray crystal structure of the major isomer was obtained (vide infra).

(f) [{Ir(CO)(dppms)(μ-I)Me}$_2$][SO$_3$CF$_3$]$_2$ (7). 4a (50 mg, 0.07 mmol) was dissolved in CH_2Cl_2 (3 cm^3) and the solution stirred under N_2. Methyl triflate (8 μL, 0.07 mmol) was added by syringe, and the solution was stirred for 30 min at room temperature. The product was recovered as a cream-white precipitate, and recrystallized as yellow blocks from CH_2Cl_2. Yield: 44 mg (72%). Anal. Calcd for ($C_{28}H_{25}F_3I_2IrO_4P_2S_2$): C, 36.3; H, 2.7; I, 13.7. Found: C, 36.1; H, 2.9; I, 13.7. IR (CH_2Cl_2): ν(CO)/cm^{-1} 2058. ^1H NMR (CD_2Cl_2): δ 8.35−7.95 (m, 20H, 7.75−7.05 arom), 5.01, 4.78, 4.65, 4.42 (each ddd, total 2H, PCH_2P for two isomers), 1.16, 1.11 (each d, total 3H, IrCH_3 for two isomers, $^3J_{HP}$ = 3 Hz). $^{31}P\{^1H\}$ NMR (CD_2Cl_2): δ 65.1 (d, *P*═S), 17.5 (d, Ir*P*, $^2J_{PP}$ = 28 Hz), 64.3 (d, *P*═S), 17.0 (d, Ir*P*, $^2J_{PP}$ = 29 Hz), 63.4 (d, *P*═S) 16.0 (d, Ir*P*, $^2J_{PP}$ = 25 Hz), 62.2 (d, *P*═S), 15.9 (d, Ir*P*, $^2J_{PP}$ = 26 Hz). The four isomers identified by NMR spectroscopy were present in a ratio of ca. 3:3:1:1. An X-ray crystal structure for an iodide-bridged dimer was obtained (vide infra).

X-ray Structure Determinations. Data were collected on either a Bruker Smart CCD area detector with an Oxford Cryostream 600 low-temperature system (complexes **5a**, **6**, and **7**) or a Siemens P4 diffractometer (complexes **3a**, **3b**, and **3c**−**NCMe**), in each case using Mo Kα radiation (λ = 0.71073 Å). The structures were solved by direct methods and refined by full-matrix least-squares methods on F^2. Hydrogen atoms were placed geometrically and refined using a riding model (including torsional freedom for methyl groups). Complex scattering factors were taken from the SHELXL program packages.[75,76] Crystallographic data are summarized in Table 7 for complexes **3b**, **6**,

(75) SHELXL97, An integrated system for solving and refining crystal structures from diffraction data: Sheldrick, G. M., University of Gottingen, Gottingen, Germany, 1997. SHELXTL, An integrated system for solving and refining crystal structures from diffraction data (Revision 5.1): Sheldrick, G. M., Bruker AXS Ltd., Madison, WI.

(76) SHELXL93, An integrated system for solving and refining crystal structures from diffraction data: Sheldrick, G. M., University of Gottingen, Gottingen, Germany, 1993.

Table 7. Summary of Crystallographic Data for Complexes **3b**, **6**, and **8**

	3b	**6**	**7**·CH_2Cl_2
empirical formula	$C_{28}H_{27}I_2OP_2Rh$	$C_{28}H_{27}I_2IrOP_2S$	$C_{29}H_{27}Cl_2F_3IIrO_4P_2S_2$
fw	798.15	919.50	1012.57
cryst syst	triclinic	monoclinic	monoclinic
space group	$P\bar{1}$	$P2_1/n$	$P2_1/n$
color	yellow	yellow	yellow
a (Å)	9.155(4)	10.2276(10)	10.7366(9)
b (Å)	10.436(4)	16.9486(17)	15.6551(13)
c (Å)	14.964(7)	17.2942(16)	20.1261(16)
α (deg)	92.53(4)	90	90
β (deg)	93.83(2)	102.196(2)	94.248(2)
γ (deg)	100.34(3)	90	90
temp (K)	293(2)	150(2)	150(2)
Z	2	4	4
final R indices	R1 = 0.0456	R1 = 0.0405	R1 = 0.0413
[$I > 2\sigma(I)$]	wR2 = 0.1117	wR2 = 0.1001	wR2 = 0.0974
R indices	R1 = 0.0653	R1 = 0.0477,	R1 = 0.0554
(all data)	wR2 = 0.1659	wR2 = 0.1074	wR2 = 0.1098
GOF	1.101	1.079	1.066

and **7**, and full listings of data are given in the Supporting Information. The structures of **3a** and **5a** were presented in a preliminary communication.[16]

Kinetic Experiments. Samples for kinetic runs were prepared by placing the required amount of freshly distilled methyl iodide in a 5 cm^3 graduated flask which was then made up to the mark with the solvent of choice (usually CH_2Cl_2). A portion of this solution was used to record a background spectrum. Another portion (typically 500 μL) was added to the solid metal complex (typically 7−8 μmol) in a sample vial to give a reaction solution with a complex concentration of ca. 15 mM. A portion of the reaction solution was quickly transferred to the IR cell, and the kinetic experiment was started. To obtain pseudo-first-order conditions, at least a 10-fold excess of MeI was used, relative to the metal complex. The IR cell (0.5 mm path length, CaF_2 windows) was maintained at constant temperature throughout the kinetic run by a thermostated jacket. Spectra were scanned in the metal carbonyl ν(CO) region (2200−1600 cm^{-1}) and saved at regular time intervals under computer control. After the kinetic run, absorbance vs time data for the appropriate ν(CO) frequencies were extracted and analyzed off-line using Kaleidagraph curve-fitting software. The decays of the bands due to **1a** (1987 cm^{-1}), **1b** (2011 cm^{-1}), **1c** (1983 cm^{-1}), **4a** (1972 cm^{-1}), and **4b** (1994 cm^{-1}) were all well fitted by exponential curves with correlation coefficients ≥0.999, to give pseudo-first-order rate constants. Each kinetic run was repeated at least twice to check reproducibility, the k_{obs} values given being averaged values with component measurements deviating from each other by ≤5%.

For kinetic experiments carried out under a pressure of CO, a high-pressure CIR cell was used to record in situ IR spectra. The CIR cell comprised a batch autoclave (Parr) modified (by SpectraTech) to accommodate a crystalline silicon CIR rod as described by Moser et al.[77] Spectra were recorded using a Perkin-Elmer 1710 FTIR spectrometer fitted with an MCT detector. The cell was mounted in an external optical bench coupled to the spectrometer. In a typical experiment, 14 mg of the iridium methyl complex [Ir(CO)(L−L)I_2Me] (L−L = dppms or dppe) was dissolved in 8 cm^3 of the required solvent and the resulting solution filtered into the CIR cell. The cell head was fitted to the body of the cell, ensuring that the stirrer was firmly tightened into the cell head. The vent lines, stirrer, and gas inlet from the cylinder were then fitted, tightened, and flushed out four times with N_2. The cell was flushed with N_2 at least four times, the last two with the stirrer on, and then heated to the required temperature. The cell was then pressurized with CO, and spectra were recorded over the range 2200−1600 cm^{-1} at regular intervals under computer control.

Computational Details. Ab intio quantum mechanical calculations using second-order Møller−Plesset (MP2) theory were performed using the Gaussian94 suite of programs.[78] Geometries of stationary points were optimized using the Berny algorithm[79] as implemented in Gaussian94. Transition states were located by employing a reaction coordinate method followed by a transition-state search based on the Berny algorithm, and characterized by frequency calculations to give Hessians with a single negative eigenvalue. We employed the LANL2DZ Gaussian basis set developed by Hay and Wadt,[80] which uses a semicore double-ζ contraction scheme for the heavy elements Rh, I, S, and P, with the light atoms C, O, and H being described by the split-valence Dunning 9-5V all-electron basis. Molecular orbitals were visualized (e.g., Figure 14) using Molekel software.[81]

Acknowledgment. This work was supported by BP Chemicals Ltd. (studentship to L.G.), the University of Sheffield, and The Royal Society. We thank Dr. D. B. Cook and Dr. P. W. Badger for advice on ab initio calculations, Prof. Luigi Cavallo for helpful discussions, and Prof. Rich Eisenberg for providing access to data prior to publication.

Supporting Information Available: Tables of kinetic data, details of crystal structure determinations (including ORTEP plots), and tables of Cartesian coordinates for optimized structures from ab initio calculations (PDF) and tables of crystal data (CIF). This material is available free of charge via the Internet at http://pubs.acs.org.

JA0176191

(77) Moser, W. R. In *Homogeneous Transition Metal Catalysed Reactions*; Moser, W. R., Slocum, D. W., Eds.; Advances in Chemistry Series, Vol. 230; American Chemical Society: Washington, DC, 1992; pp 3−18.
(78) Gaussian 94, Revision D.4: Frisch, M. J.; Trucks, G. W.; Schlegel, H. B.; Gill, P. M. W.; Johnson, B. G.; Robb, M. A.; Cheeseman, J. R.; Keith, T.; Petersson, G. A.; Montgomery, J. A.; Raghavachari, K.; Al-Laham, M. A.; Zakrzewski, V. G.; Ortiz, J. V.; Foresman, J. B.; Cioslowski, J.; Stefanov, B. B.; Nanayakkara, A.; Challacombe, M.; Peng, C. Y.; Ayala, P. Y.; Chen, W.; Wong, M. W.; Andres, J. L.; Replogle, E. S.; Gomperts, R.; Martin, R. L.; Fox, D. J.; Binkley, J. S.; Defrees, D. J.; Baker, J.; Stewart, J. P.; Head-Gordon, M.; Gonzalez, C.; Pople, J. A., Gaussian, Inc., Pittsburgh, PA, 1995.
(79) Schlegel, H. B. *J. Comput. Chem.* **1982**, *3*, 214.
(80) Hay, P. J.; Wadt, W. R. *J. Chem. Phys.* **1985**, *82*, 270. Hay, P. J.; Wadt, W. R. *J. Chem. Phys.* **1985**, *82*, 299. Wadt, W. R.; Hay, P. J. *J. Chem. Phys.* **1985**, *82*, 284.
(81) MOLEKEL (4.0): Flukiger, P.; Luthi, H. P.; Portmann, S.; Weber, J., Swiss Center for Scientific Computing, Manno, Switzerland, 2000.